

Natural MSSM after the LHC 8 TeV run

Kamila Kowalska and Enrico Maria Sessolo

National Centre for Nuclear Research, Hoża 69, 00-681 Warsaw, Poland

Kamila.Kowalska@fuw.edu.pl, Enrico-Maria.Sessolo@fuw.edu.pl

Abstract

We investigate the impact of direct LHC SUSY searches on the parameter space of three natural scenarios in the MSSM. In the first case the spectrum consists of light stops, sbottoms, and Higgsino-like neutralinos, while the other particles are assumed to be out of the experimental reach. In the second case we consider an additional light gluino. Finally we study a more complex spectrum comprising also light sleptons, wino-like chargino, and a bino-like neutralino. We simulate in detail three LHC searches: stop production at ATLAS with 20.7/fb, CMS 11.7/fb inclusive search for squarks and gluinos with the variable α_T , and CMS 9.2/fb electroweak production with 3 leptons in the final state. For each point in our scans we calculate the exclusion likelihood due to the individual searches and to their statistical combination. We calculate the fine-tuning measure of the points allowed by the LHC and the implications for the Higgs mass and other phenomenological observables: the relic density, $\text{BR}(B_s \rightarrow \mu^+ \mu^-)$, $\text{BR}(\bar{B} \rightarrow X_s \gamma)$, and the spin-independent neutralino-proton scattering cross section. We find that points with acceptable levels of fine tuning are for the most part already excluded by the LHC and including the other constraints further reduces the overall naturalness of our scenarios.

1 Introduction

With the end of 2012, the LHC completed its $\sqrt{s} = 8\text{ TeV}$ run, and both the ATLAS and CMS collaborations collected approximately 21/fb of data. Many physics analyses have been already completed and made public by the two collaborations, in the framework of the Standard Model (SM) and beyond (BSM). Additional analyses are scheduled to appear in the next few months. Undoubtedly, the greatest success has been the observation of the Higgs boson of the SM [1, 2], or at least of a particle that couples to the SM with very similar strength, with mass $m_h \simeq 125\text{ GeV}$. On the other hand, direct searches for new BSM physics, which in the largest share are designed for the observation of low energy supersymmetry (SUSY), have given null results to this point.

In the context of SUSY the latest LHC results just mentioned (the discovery of the Higgs boson, the non-observation of light SUSY particles, but also the first evidence of a SM-like BR ($B_s \rightarrow \mu^+ \mu^-$) at LHCb [3]) seem to point to the fact that within the framework of the Minimal Supersymmetric Standard Model (MSSM) the typical scale of the superpartners, defined as the geometric mean of the stop masses, $M_{\text{SUSY}} = (m_{\tilde{t}_1} m_{\tilde{t}_2})^{1/2}$, is higher than the scale presently testable with direct searches. In fact, in the MSSM, $m_h \simeq 125\text{ GeV}$ requires stops in the multi-TeV regime, unless one accounts for nearly maximal stop mixing, $|X_t|/M_{\text{SUSY}} \simeq \sqrt{6}$ [4, 5, 6]. While this fact does not pose any particular problem from the phenomenological point of view (see, e.g., [7] for a recent global analysis), the implications of large M_{SUSY} have exacerbated the “naturalness” problem of the MSSM, also called in the literature the “Little Hierarchy” problem [8, 9], i.e. the requirement that the electroweak (EW) scale be obtained without excessive fine-tuning of the soft SUSY-breaking terms in the Lagrangian.

To put the issue in more quantitative terms, let us consider a measurement of fine-tuning for the soft SUSY-breaking terms (here generically indicated with p_i) that enter the minimization conditions of the scalar potential: for instance the well known Barbieri-Giudice measure [8], $\Delta = \max \Delta_{p_i}$, with

$$\Delta_{p_i} = \left| \frac{\partial \log M_Z^2}{\partial \log p_i^2} \right|. \quad (1)$$

One can calculate Δ (by using, e.g., the formulas of [10]) for the values of the soft terms that are favored at 2σ by the Higgs mass measurement. The obtained fine-tuning depends on the scale of the SUSY-breaking sector, Λ : if $\Lambda = 10\text{ TeV}$ one gets $\Delta \sim 40\text{--}100$ for $m_{\tilde{t}_1}, m_{\tilde{t}_2} \sim 600\text{--}1000\text{ GeV}$ and maximal stop mixing (provided μ does not exceed $500\text{--}600\text{ GeV}$), and $\Delta \simeq 200$ or more for $m_{\tilde{t}_1}, m_{\tilde{t}_2} > 3000\text{ GeV}$ with zero mixing; if, on the other hand, $\Lambda \sim 10^{16}\text{ GeV}$, then Δ increases by an order of magnitude or more, depending on the value of the gluino mass (although for very large Λ the leading log (LL) approximation must be taken with caution [11]).

Thus, in the MSSM the measured value of the Higgs mass requires a large amount of fine-tuning. (Addition of extra sectors, like in the case of the Next-to-Minimal Supersymmetric SM can ameliorate this problem by raising the value of the tree-level Higgs mass [12].) On the other hand, since Δ is generally larger in the case with multi-TeV stop masses than in the case where the correct Higgs mass is obtained thanks to maximal stop mixing, in the last couple of

years the idea of Natural SUSY [10, 13, 14, 15, 16, 17] has emerged in the literature, whose spectra are characterized by the presence of light stops and sbottoms – which are not as much constrained by the LHC searches as the first two generations’ squarks –, by a small value of the μ parameter, and by heavy masses for the remaining squarks. Interestingly, ATLAS and CMS have followed this lead, and their interpretations of the results from direct SUSY searches have shifted from being heavily oriented towards constrained models like the Constrained MSSM [18], to simplified models (SMS) [19] designed to exclude particles more in line with the naturalness requirement.

The exclusion bounds obtained in the framework of the SMS, however, cannot be applied straightforwardly to more general scenarios for several reasons. First, in a SMS strong assumptions are made about the nature of the particles produced, as well as their decay chains. A single decay chain is usually considered, with the corresponding branching ratios (BR) set to 100%. In principle, then, for a general model the presence of intermediate particles can result in softer decay chains that can reduce the signal, so that the power of the search is weakened. This was observed for some points in [7], where the statistical impact of two LHC SUSY searches, the CMS α_T search with 11.7/fb integrated luminosity [20] and the CMS 3-lepton search for EW production [21], was calculated on the parameter space of a 9-dimensional parametrization of the MSSM. Secondly, additional constraints are generally put on the masses of SUSY particles that appear at intermediate steps in the decay chain. These do not need to be satisfied in a more complex model.

On the other hand, a detailed simulation of a LHC search for a complex model can produce limits on a certain particle’s mass that are enhanced with respect to the ones obtained in a SMS involving the same particle. This could be due to the presence of two (or more) particles producing indistinguishable signatures at the detector level, as recently shown in [17], where a LHC analysis of Natural SUSY-type of spectra involving light μ , \tilde{t}_L , \tilde{b}_L , and \tilde{t}_R was performed. Or, if all available production channels are open, additional limits on the mass of a certain particle can be put indirectly by the production and decay of a different particle if the spectra show some correlation. This issue has been discussed in [16] in the context of bounds on third generation squarks and on gluinos, where also the necessity of combining different experimental signatures was emphasized.

In this paper, following the procedure for the implementation of LHC SUSY searches adopted in [7], we perform a similar analysis for three MSSM scenarios, whose spectra are natural in the sense described by Eq. (1). We consider the following cases, ordered with increasing complexity in the spectrum: 1. The spectrum consists of light \tilde{t}_1 , \tilde{b}_1 , \tilde{t}_2 , and Higgsino-like neutralinos; 2. The spectrum includes also light gluinos; 3. The spectrum consists of the same particles as in Scenario 2, with the exception that the lightest neutralino is bino-like, the lightest chargino is wino-like, and there are light sleptons.

For each scenario we generate a random sample of points. For each point we perform on-the-fly simulation of the LHC signal, from generation of the hard scattering events to simulation of the detector’s response to calculate the efficiencies (see also [22, 23, 24, 25] for a description

of this procedure), and compare the signal to the observed and background yields, provided by the experimental collaborations, through construction of a likelihood function. We consider three LHC searches, based on the $\sqrt{s} = 8 \text{ TeV}$ data-set: 21/fb ATLAS direct stop production with 1 lepton in the final state [26] and the two searches that were already used in [7]: 9.2/fb CMS 3-lepton EW production and 11.7/fb CMS α_T inclusive search. However, we updated the procedure of [7] by including the next-to-leading-order and next-to-leading-log (NLO+NLL) corrections to the production cross-sections. We then consider statistical combinations of the implemented searches for our three scenarios and derive combined limits on the sparticle masses. This is similar in spirit to the procedure adopted in [16], which used some of the CMS searches from the $\sqrt{s} = 7 \text{ TeV}$ data-set. Finally, for the points in our scenarios that are not excluded at the 95% C.L. we calculate the fine-tuning measure according to Eq. (1), as well as some relevant phenomenological observables: Higgs mass, relic density, $\text{BR}(\bar{B} \rightarrow X_s \gamma)$, $\text{BR}(B_s \rightarrow \mu^+ \mu^-)$, and the spin-independent (SI) neutralino-proton scattering cross section, σ_p^{SI} .

We limit ourselves to regions of the parameter space over which the LHC searches we simulate have significant sensitivity. This means that we do not treat here the case of compressed spectra, for which $|m_{\tilde{t}, \tilde{b}, \tilde{g}} - m_{\tilde{\chi}_1^0}|/m_{\tilde{t}, \tilde{b}, \tilde{g}} \ll 1$. It is known that those regions are “pockets” in which Natural SUSY could be hiding [17].

Our analysis presents elements in common with the works mentioned above, Refs. [16] and [17], but we also show several novel features: 1) The LHC searches we select involve third generation squarks, gluinos, and EW-produced charginos and neutralinos, and they are all based on the $\sqrt{s} = 8 \text{ TeV}$ data set; 2) We consider very general, R -parity conserving, loosely natural MSSM spectra to analyze some interesting effects (limits from EW production, decays of gluinos and third generation squarks through off- and on-shell sleptons); 3) We quantify the fine-tuning for all our points and analyze the impact of phenomenological constraints other than the direct searches at the LHC.

This paper is organized as follows. In Sec. 2 we summarize the features of natural MSSM spectra and we define the three scenarios considered in this analysis. In Sec. 3 we describe our procedure for deriving the likelihood functions for direct SUSY searches at the LHC and we present the results of their validation against the official limits from ATLAS and CMS. Section 4 is devoted to the discussion of the results. We summarize our findings in Sec. 5.

2 Naturalness in the MSSM

The concept of Natural SUSY is closely related to the EW symmetry breaking mechanism and has been widely discussed in the literature. Here we briefly recall its most important features.

One of the minimization conditions of the scalar potential allows to express the mass of the Z boson in terms of the running soft terms m_{H_u} , m_{H_d} and μ ,

$$\frac{1}{2}M_Z^2 = -\mu^2 + \frac{(m_{H_d}^2 + \Sigma_d) - (m_{H_u}^2 + \Sigma_u) \tan^2 \beta}{\tan^2 \beta - 1}, \quad (2)$$

where Σ_u and Σ_d are the radiative corrections to the tree-level potential, which depend on the

SUSY mass spectrum. For moderate to large $\tan\beta$ ($\tan\beta > 8$), the m_{H_d} term can be neglected and the correct value of M_Z is obtained through the cancellation between the μ^2 , $m_{H_u}^2$ and Σ_u terms. The naturalness criterion [8] states that μ^2 and Σ_u should be of the order of the EW symmetry breaking scale (squared), in order to avoid excessive, or “unnatural” fine-tuning of the model parameters.

A widely used measure of the EW fine-tuning associated with the parameters of the model is given in Eq. (1). The total measure Δ for a given model point is the maximal contribution to the fine-tuning among all of the model point parameters. A precise determination of the amount of fine-tuning that makes a model unnatural is somewhat a matter of taste. In the literature it is usually assumed that a viable amount is $\Delta^{-1} \sim 10 - 20\%$.

In this paper we will be more conservative, and assume an upper bound for our generated spectra $\Delta^{-1} \geq 1\%$, or $\Delta \leq 100$. We can easily translate this requirement into upper bounds for the soft terms [10]. From Eq. (2) one can see that the μ parameter cannot exceed M_Z by order of magnitudes, which implies fairly light Higgsinos. By calculating the measure of Eq. (1) from Eq. (2) and imposing $\Delta \leq 100$ one gets

$$|\mu| \lesssim 645 \text{ GeV} . \quad (3)$$

Secondly, since the dominant loop contribution to Σ_u comes from the top Yukawa and from squarks of the third generation running in the loop, and it is given in the LL approximation by [27, 10]

$$\Sigma_u|_{\text{stop}} = -\frac{3y_t^2}{8\pi^2}(m_{\tilde{Q}_3}^2 + m_{\tilde{u}_3}^2 + |A_t|^2) \log\left(\frac{\Lambda}{\text{TeV}}\right) , \quad (4)$$

imposing $\Delta \leq 100$ places a direct constraint on the third generation soft masses and mixing,

$$(m_{\tilde{Q}_3}^2 + m_{\tilde{u}_3}^2 + |A_t|^2) \lesssim (3700 \text{ GeV})^2 \log\left(\frac{\Lambda}{\text{TeV}}\right)^{-1} , \quad (5)$$

where Λ is the scale at which SUSY breaking is transmitted to the MSSM. (The bounds become increasingly more severe when raising Λ by orders of magnitude above the TeV scale.)

The one-loop contribution to Eq. (2) due to a Majorana wino reads

$$\Sigma_u|_{M_2} = -\frac{3g_2^2}{8\pi^2}|M_2|^2 \log\left(\frac{\Lambda}{\text{TeV}}\right) , \quad (6)$$

so that $\Delta \leq 100$ gives

$$|M_2| \lesssim 5400 \text{ GeV} \cdot \log\left(\frac{\Lambda}{\text{TeV}}\right)^{-1/2} . \quad (7)$$

Finally, the contribution from a Majorana gluino to the stop mass can be significant, introducing a non-negligible two-loop contribution to the Σ_u term,

$$\Sigma_u|_{M_3} = -\frac{2y_t^2}{\pi^3}\alpha_s|M_3|^2 \log^2\left(\frac{\Lambda}{\text{TeV}}\right) . \quad (8)$$

One gets, for the gluino mass parameter M_3 ,¹

$$|M_3| \lesssim 8500 \text{ GeV} \cdot \log\left(\frac{\Lambda}{\text{TeV}}\right)^{-1} . \quad (9)$$

¹In the case of Dirac gluinos the limit is weaker [28, 10].

Scenario 1	Scenario 2	Scenario 3
$M_1 = 3 \text{ TeV}$	$M_1 = 3 \text{ TeV}$	$0.01 \text{ TeV} \leq M_1 \leq 0.4 \text{ TeV}$
$M_2 = 1.5 \text{ TeV}$	$M_2 = 1.5 \text{ TeV}$	$M_1 < M_2$
$M_3 = 1.6 \text{ TeV}$	$0.1 \text{ TeV} \leq M_3 \leq 1.6 \text{ TeV}$	$0.1 \text{ TeV} \leq M_2 \leq 0.63 \text{ TeV}$
$m_{\tilde{L}_{1,2,3}} = m_{\tilde{e}_1} = m_{\tilde{e}_2} = m_{\tilde{e}_3} = 3 \text{ TeV}$	$m_{\tilde{L}_{1,2,3}} = m_{\tilde{e}_1} = m_{\tilde{e}_2} = m_{\tilde{e}_3} = 3 \text{ TeV}$	$0.1 \text{ TeV} \leq M_3 \leq 1.6 \text{ TeV}$
$0.075 \text{ TeV} \leq \mu \leq 0.63 \text{ TeV}$	$0.075 \text{ TeV} \leq \mu \leq 0.63 \text{ TeV}$	$0.1 \text{ TeV} \leq m_{\tilde{L}_{1,2,3}}, m_{\tilde{e}_1}, m_{\tilde{e}_2}, m_{\tilde{e}_3} \leq 0.63 \text{ TeV}$
$0.1 \text{ TeV} \leq m_{\tilde{Q}_3}, m_{\tilde{u}_3} \leq 1.4 \text{ TeV}$	$0.1 \text{ TeV} \leq m_{\tilde{Q}_3}, m_{\tilde{u}_3} \leq 1.4 \text{ TeV}$	$\mu = 0.63 \text{ TeV}$
$\tilde{t}_{1,2}, \tilde{b}_1, \tilde{\chi}_1^0, \tilde{\chi}_2^0, \tilde{\chi}_1^\pm$	$\tilde{g}, \tilde{t}_{1,2}, \tilde{b}_1, \tilde{\chi}_1^0, \tilde{\chi}_2^0, \tilde{\chi}_1^\pm$	$0.1 \text{ TeV} \leq m_{\tilde{Q}_3}, m_{\tilde{u}_3} \leq 1.4 \text{ TeV}$
		sleptons, $\tilde{g}, \tilde{t}_{1,2}, \tilde{b}_1, \tilde{\chi}_1^0, \tilde{\chi}_2^0, \tilde{\chi}_1^\pm$

Table 1: Soft SUSY-breaking parameters characteristic of the natural scenarios considered in this study. The bottom line shows the light particles present in each spectrum.

The other particles in the spectrum can either have a much larger mass (masses of the squarks of the first two generations are already pushed well above 1 TeV by the limits from direct SUSY searches at the LHC), or allowed to be at the same mass scale as the light ones. Such a possibility is particularly interesting in the case of sleptons, since it opens a way of testing a model with direct EW production of charginos and neutralinos. On the other hand, allowing different compositions for the lightest neutralino (by assuming $M_1, M_2 < \mu$) would allow to investigate different scenarios for generating the dark matter in the Universe.

As mentioned in Sec. 1, we construct three scenarios in the MSSM, with characteristic spectra subject to the bounds of Eqs. (3)-(9). We randomly scan the parameters of the phenomenological MSSM (parametrized in its unconstrained version by 24 free parameters defined at M_{SUSY}), on which we impose conditions leading to natural spectra. We assume that the squarks of the first two generations are out of reach at the LHC, $m_{\tilde{Q}_{1,2}} = m_{\tilde{u}_1} = m_{\tilde{u}_2} = m_{\tilde{d}_1} = m_{\tilde{d}_2} = 5 \text{ TeV}$. Similarly, we set $m_{\tilde{d}_3} = 5 \text{ TeV}$, and fix $A_b = A_\tau = -0.5 \text{ TeV}$. $A_t, \tan \beta, m_A$ are free to vary in the following ranges: $-2 \text{ TeV} \leq A_t \leq 2 \text{ TeV}$, $3 \leq \tan \beta \leq 62$, $0.1 \text{ TeV} \leq m_A \leq 2 \text{ TeV}$. The scanning ranges of the remaining parameters are summarized for each scenario in Table 1. Where relevant, we impose LEP limits [29] on the masses of charginos, sleptons and neutralinos. Notice that, given our choices for M_3 and M_2 , the fine-tuning measure associated with those parameters is always $\Delta_{M_{2,3}} \lesssim 5$ (for $\Lambda \simeq 10 \text{ TeV}$), so that the main contribution to the total Δ comes from the third generation squarks and Higgsino sector. Notice also that we do not make any additional assumptions about the mass hierarchy between the light sparticles, as well as the mixing in the stop sector. We differ in this from [16] and [17]. Finally, our choice of gaugino mass parameters in Scenario 3 will allow us to investigate the impact of the LHC searches in the EW sector.

For each scenario we create a sample of more than 5000 points, the vast majority of which satisfy the constraints on the Higgs mass, $\text{BR}(\bar{B} \rightarrow X_s \gamma)$, and $\text{BR}(B_s \rightarrow \mu^+ \mu^-)$ at 2σ , where the central values and uncertainties are given in Table 2 of Ref. [7]. We find that the points

that, in a way or another, do not fall in the 2σ window lie in the very low mass range of the spectra tested at the LHC and will be easily excluded by the direct SUSY limits. Since the main focus of this paper is to analyze the impact of LHC searches on the spectra, we include these points when showing our results in Sec. 4.

For the relic density we impose only an upper limit at 2σ , as it is well known that small Higgsino masses tend to create an underabundance of present-day dark matter with respect to the central value measured by PLANCK [30] or WMAP [31]. This is not necessarily a problem for the model, since it is easy to conceive plausible mechanisms and additional particles that can boost the value of the relic density, as explained, e.g., in [32] and references therein.

The mass spectra are calculated with `softsusy-3.3.6` [33], $\text{BR}(\bar{B} \rightarrow X_s \gamma)$ and $\text{BR}(B_s \rightarrow \mu^+ \mu^-)$ with `superiso v3.3` [34], the relic density and σ_p^{SI} with `MicrOMEGAs 2.4.5` [35]. The numerical codes are interfaced through the package BayesFITS, described in detail in [23, 24, 7].

3 LHC SUSY limits

In this section we describe our implementation of the LHC SUSY limits. To validate the accuracy of our procedure, we also show here the results of applying the searches to some of the SMS designed by the experimental collaborations.

We extend the procedure developed in [7]. For each implemented search we construct an approximate but accurate likelihood function, which yields an exclusion C.L. for each point in our samples. The likelihood is obtained through an algorithm that mimics the analyses performed by the experimental collaborations. For every point in the parameter space we calculate the decay branching ratios with `SUSYHIT` [36], generate 5000 events at the scattering level with `PYTHIA6.4` [37], and pass the hadronization products to the fast detector simulator `PGS4` [38]. From the physical objects produced by the detector simulator, we construct the kinematical variables, α_T , H_T , M_T , m_{eff} , am_{T_2} , m_{jjj} , proper of the three searches considered here (described below) and apply the selection cuts. We use the CMS and ATLAS detector cards respectively, with the settings recommended by both collaborations. We also tune the b -tagging algorithm used by `PGS4` in order to reproduce the corresponding efficiencies reported by CMS [39] and ATLAS [40]. This step is particularly important, since b -tagging plays a crucial role in deriving the exclusion bounds for the squarks of the third generation. Finally, different kinematical bins i are constructed, closely following the experimental papers, the cuts are applied and the acceptances/efficiencies ε_i are calculated as the fraction of events that pass all the cuts. We use NLO+NNL cross-sections, $\sigma_{\text{NLO+NNL}}$, provided by LHC SUSY Cross Section Working Group [41].

The number of signal events in a given bin is calculated as $s_i = \varepsilon_i \times \sigma_{\text{NLO+NNL}} \times \int L$, where $\int L$ is the integrated luminosity. The obtained signal yields are finally statistically compared to the publicly available observed (o_i) and background (b_i) yields of the searches, provided in the experimental papers, as described in [23, 25]. The systematic uncertainties on the background yields (δb_i) are accounted for in our analysis by convolving the Poisson distribution P with a

Gaussian or log-normal (depending on the bin [23]) distribution G . The likelihood function for each bin is thus calculated,

$$\mathcal{L}_i(o_i, s_i, b_i) = \int P(o_i|s_i, \bar{b}_i) G(\bar{b}_i|b_i, \delta b_i) d\bar{b}_i, \quad (10)$$

and the final likelihood for each point is the product of the likelihoods for each separate bin. The appropriate C.L. is obtained from the $\delta\chi^2$ variable as $\delta\chi^2 = -2\log(\mathcal{L}/\mathcal{L}_{\max})$.

Both ATLAS and CMS performed many analyses at $\sqrt{s} = 8$ TeV with different experimental signatures. For the purpose of this paper, we implement the analyses that either present the strongest exclusion limits on the mass of a particle under study,² or are more general in the sense that can constrain different types of particles. Below we present a brief summary of our strategy for each search and the results of the validation.

3.1 ATLAS 1 lepton + 4(1b-) jets + E_T^{miss} , 21/fb

To constrain our scenarios with limits from direct stop production searches we simulate the ATLAS 1 lepton + 4(1b-) jets + missing energy (MET) search with 20.7/fb [26]. The 95% C.L. exclusion bound in the $(m_{\tilde{t}}, m_{\tilde{\chi}_1^0})$ plane for a SMS of direct stop production with $BR(\tilde{t}_1 \rightarrow t + \tilde{\chi}_1^0) = 100\%$ (here after called SMS TN) shown in [26] is comparable to the ones obtained with ATLAS all hadronic searches for direct stop and stop/sbottom production with 20.5/fb and 20.1/fb, respectively [43, 44]. It is also comparable to the one given by the CMS 1-lepton + jets + MET search with 19.5/fb [45]. The bounds of [26] are instead significantly stronger than the ones produced with the ATLAS 2-leptons + jets + MET search with 20.3/fb [46]. The observed and background yields that we use for our simulation, together with the systematic uncertainties are given in Tables 2, 3, and 4 of Ref. [26].

As a form of validation, we applied our simulation to a sample of 5000 points for which the only light SUSY particles were \tilde{t}_1 and a bino-like neutralino. This was meant to reproduce SMS TN, for which the ATLAS collaboration provides a 95% C.L. bound in the $(m_{\tilde{t}}, m_{\tilde{\chi}_1^0})$ plane. The result of our validation is given in Fig. 1(a). Gray dots represent the points excluded by our likelihood function at the 99.7% C.L., cyan diamonds are excluded at the 95.0% C.L., and blue triangles are excluded at the 68.3% C.L. The points depicted as red squares are considered as allowed. The solid black line shows the 95% C.L. ATLAS exclusion limit, which we present for comparison.

3.2 CMS 3 leptons + E_T^{miss} , 9/fb

To constrain our scenarios with limits from direct production of charginos and neutralinos we simulate the CMS, 3 leptons + MET, EW production search with 9.2/fb [21]. Notice that the 95% C.L. exclusion bounds published by CMS for the $(m_{\tilde{\chi}_1^\pm}, m_{\tilde{\chi}_1^0})$ plane are comparable to the

²In the days preceding the submission of this paper the CMS Collaboration updated the results of the EW search to 19.5/fb [42]. While the limits from EW production in Scenario 3 will become even more severe, we do not expect significant qualitative differences for the results presented in Sec. 4.

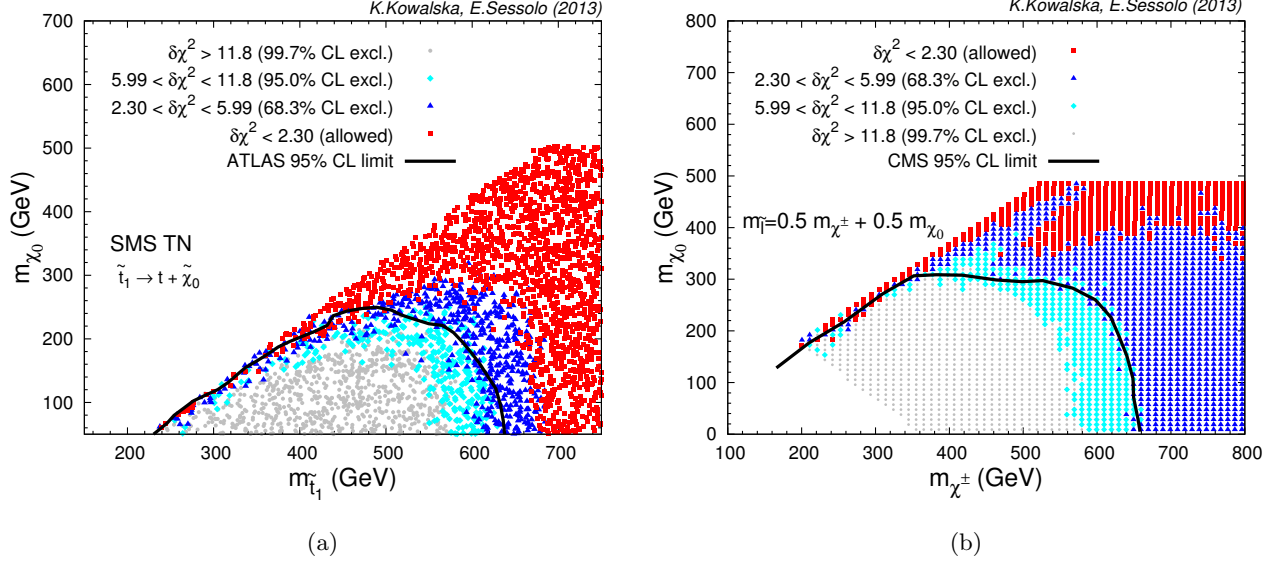


Figure 1: (a) Our simulation of the ATLAS 1-lepton search for direct stop production applied to SMS TN. (b) Our simulation of the CMS 3-lepton search for EW production applied to a SMS with $m_{\tilde{t}} = 0.5 m_{\tilde{\chi}_1^\pm} + 0.5 m_{\tilde{\chi}_1^0}$. Points that are excluded at the 99.7% C.L. are showed as gray dots, at the 95.0% C.L. as cyan diamonds, and at the 68.3% C.L. as blue triangles. The points shown as red squares are considered as allowed. The solid black lines show the published 95% C.L. contours by ATLAS and CMS, which we use for comparison.

ones obtained by the ATLAS 3 leptons + MET search with 20.7/fb [47], given equivalent SMS, and are stronger than the bounds on the same masses obtained by the ATLAS di-lepton search with 20.3/fb [48].

The details of our simulation are given in [7]. We repeat that we here updated the cross section to the NLO+NLL to increase the accuracy of our calculation. We limit ourselves to final states with a ee or $\mu\mu$ opposite-sign pair where the third lepton is either an electron or a muon, which is the box giving the strongest constraints. The observed and background yields and the systematic uncertainties are given in Table 1 of [21]. To validate our likelihood function, we generated a sample of 2500 points where the only light particles in the spectrum were wino-like $\tilde{\chi}_1^\pm$ and $\tilde{\chi}_2^0$, a bino-like $\tilde{\chi}_1^0$, and unified sleptons with mass $m_{\tilde{t}} = 0.5 m_{\tilde{\chi}_1^\pm} + 0.5 m_{\tilde{\chi}_2^0}$. This was meant to reproduce one of the SMS for which CMS provided a 95% C.L. exclusion bound in the $(m_{\tilde{\chi}_1^\pm}, m_{\tilde{\chi}_1^0})$ plane. The exclusion plot for this SMS is presented in Fig. 1(b). The color code is the same as in Fig. 1(a). The black solid line represent the 95% C.L. exclusion limit by CMS, which we show for comparison.

3.3 CMS 0 leptons + (b-) jets + E_T^{miss} with α_T , 12/fb

We implement the bounds on direct production of gluinos, sbottoms and stops with 0 leptons in the final state by simulating the CMS α_T search with 11.7/fb [20].

The search employs a set of 8 different boxes, with hard jets and MET in the final states,

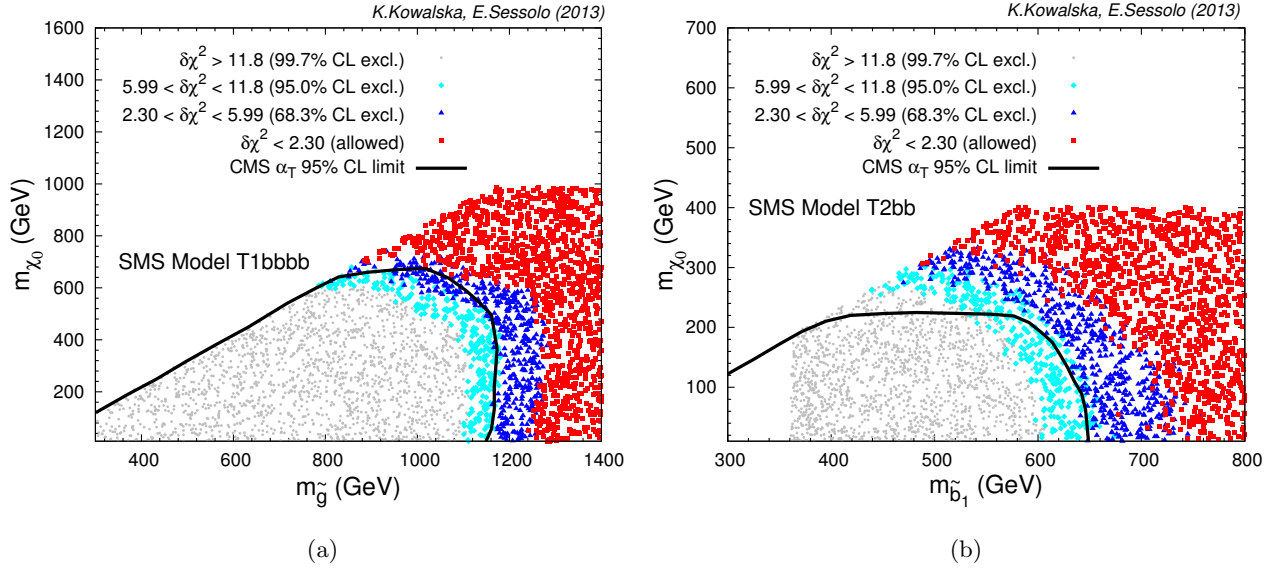


Figure 2: Our simulation of the CMS α_T search in (a) SMS T1bbbb, and (b) SMS T2bb. The color code is the same as in Fig. 1. The solid black lines show the published 95% C.L. contours by CMS, which we use for comparison.

and different combinations of b -tagged jets. It is therefore sensitive to events with different topologies. For the purpose of this paper we are interested in stop/sbottom production, and production of gluinos decaying to squarks of the third generation. The boxes, together with the number of the observed and background events provided by the CMS Collaboration, are given in [49].

We use this search because of its versatility, and still the bounds obtained in the framework of different SMS are among the most constraining in the literature. In particular, for gluinos decaying to stops, the bounds are comparable to the ones from the CMS HT , b -jets and MET search with 19.4/fb [50] and, for $m_{\tilde{\chi}_1^0} \lesssim 400$ GeV, to the bounds from the opposite-sign leptons + b -jets searches at CMS and ATLAS [39, 51] and the 3-lepton + b -jets search with 19.5/fb at CMS [52]. However, in this topology, the searches of Refs. [39, 51, 52] are more constraining than the α_T search in the $400 \text{ GeV} \lesssim m_{\tilde{\chi}_1^0} \lesssim 600 \text{ GeV}$ range. The CMS single-lepton + (b -) jets search with 19.4/fb [53] and the ATLAS 0-lepton + jets + MET search with 20.3/fb [54] are instead more constraining than the α_T search by about 200 GeV for a small neutralino mass. For gluinos decaying to sbottoms the bounds from the α_T search are the strongest in the literature, comparable to the ones from the CMS HT , b -jets and MET search. For direct sbottom production, the bounds are among the strongest and comparable to the bounds from the ATLAS 0-lepton + 2 b -jets + MET search with 20.1/fb [44].

Our implementation of the α_T search is described in detail in [25, 7], with the difference that we here updated the cross section to the NLO+NLL.

We validated our simulation for direct gluino production on a sample of 5000 points whose spectra presented gluinos, \tilde{b}_1 , and bino-like neutralinos as the sole light particles. This was

meant to mimic SMS T1bbbb for which the CMS Collaboration provided a 95% C.L. exclusion bound in the $(m_{\tilde{g}}, m_{\tilde{\chi}_1^0})$ plane. The result of our calculation, compared to the CMS bound, is shown in Fig. 2(a).

For direct sbottom production we applied the simulation to a sample of points with only light \tilde{b}_1 and bino-like neutralinos, in order to mimic SMS T2bb. The result, in the $(m_{\tilde{b}_1}, m_{\tilde{\chi}_1^0})$ plane, is shown in Fig. 2(b). The color code is the same as in Fig. 1. One can see that our likelihood does not reproduce the CMS bound to the desired accuracy in the region with $m_{\tilde{\chi}_1^0} > 200$ GeV. We thus remind the reader that our methodology gives only a good approximation and is not meant to replace the official bounds, which are calculated much more precisely by the experimental collaborations.

4 Results

In this section we show the impact of the three LHC SUSY searches on the parameter space of our scenarios. Our conclusions will always be drawn with respect to the 95% C.L. bounds obtained from our likelihood function. However, as mentioned at the end of Sec. 3.3, our procedure is an approximation subject to some uncertainty. We show in our plots the 68.3% C.L. and 99.7% C.L., which can be loosely interpreted as an estimate of the uncertainty associated with our calculation.

We also calculate in this section the level of fine-tuning for each scenario and discuss the implications of the LHC bounds on some phenomenological observables: the Higgs mass, $m_h \simeq 125$ GeV, the relic density, $\text{BR}(\text{B}_s \rightarrow \mu^+ \mu^-)$, $\text{BR}(\overline{\text{B}} \rightarrow \text{X}_s \gamma)$, and σ_p^{SI} .

4.1 Scenario 1

As discussed in Sec. 2, Scenario 1 is the one characterized by the smallest number of light SUSY particles. The spectra include light $\tilde{t}_{1,2}$, \tilde{b}_1 , and Higgsino-like, almost degenerate $\tilde{\chi}_1^0$, $\tilde{\chi}_2^0$, and $\tilde{\chi}_1^\pm$.

Obviously, the three searches we selected have different constraining power on the produced spectra. The ATLAS 1-lepton search is sensitive to stop and sbottom pair production. The gluinos are too heavy in this scenario, $m_{\tilde{g}} > 1730$ GeV, to be produced in significant numbers. The charginos and neutralinos, on the other hand, are degenerate so that production of top quarks via processes like $\tilde{\chi}_1^\pm \rightarrow W^\pm \tilde{\chi}_1^0$ or $\tilde{\chi}_2^0 \rightarrow Z \tilde{\chi}_1^0$ is highly suppressed.

The limits on \tilde{t}_1 are mainly obtained through the $\tilde{t}_1 \rightarrow t \tilde{\chi}_1^0$ chain, which gives the largest efficiency, and the exclusion plot in the $(m_{\tilde{t}_1}, m_{\tilde{\chi}_1^0})$ plane looks very similar to Fig. 1(a), with only a slightly increased presence of excluded points above the limit obtained in SMS TN. This is due to the presence of light sbottoms, which can decay through $\tilde{b}_1 \rightarrow t \tilde{\chi}_1^-$, where the chargino is invisible since it decays softly to the lightest neutralino.

It is then interesting to notice that in Scenario 1 the ATLAS 1-lepton search can place a strong 95% C.L. exclusion bound on the mass of the lightest sbottom, which can be inferred in the $(m_{\tilde{b}_1}, m_{\tilde{\chi}_1^0})$ plane from the boundary region between the cyan diamonds and blue triangles

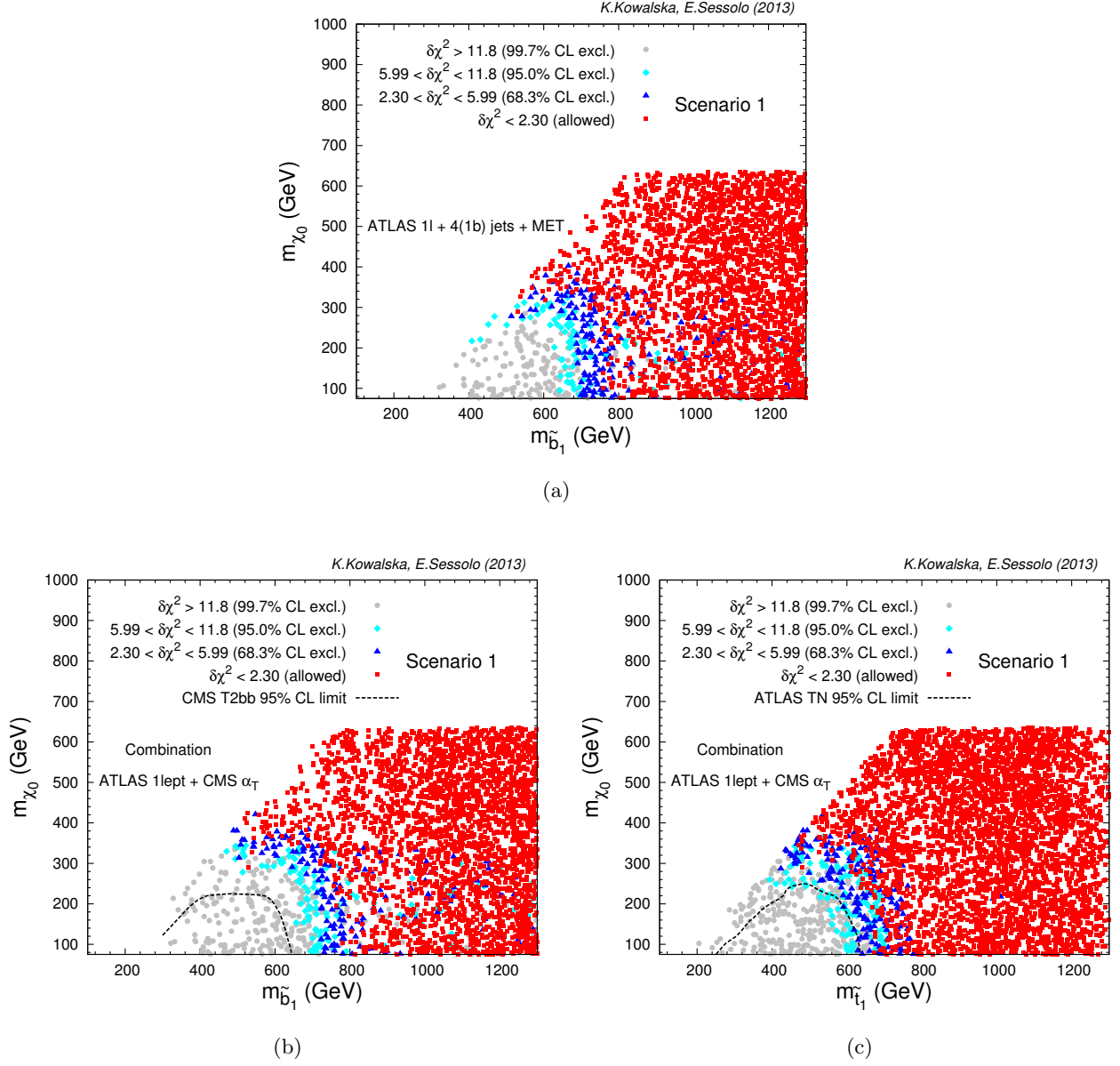


Figure 3: (a) Exclusion levels in the $(m_{\tilde{b}_1}, m_{\tilde{\chi}_1^0})$ plane from our simulation of the ATLAS 1-lepton search in Scenario 1. (b) Exclusion levels in the $(m_{\tilde{b}_1}, m_{\tilde{\chi}_1^0})$ plane from our combination of the ATLAS 1-lepton and CMS α_T searches. The dashed black line show the published CMS α_T 95% C.L. bound in SMS T2bb. (c) Exclusion levels in the $(m_{\tilde{t}_1}, m_{\tilde{\chi}_1^0})$ plane from our combination of the ATLAS 1-lepton and CMS α_T searches. The dashed black line show the published ATLAS 95% C.L. bound in SMS TN. The color code is the same as in Fig. 1.

in Fig. 3(a). The light sbottoms are excluded in two different ways: either directly, via the $\tilde{b}_1 \rightarrow t\chi_1^-$ decay chain, as mentioned above, or through the exclusion of stops, which in this scenario are lighter than the sbottoms.

For final states *without* an isolated lepton with $p_T > 25$ GeV (as required by the ATLAS search [26]), the CMS α_T search can place strong bounds on the mass of the stops and sbottoms.

We want to point out here that, while our simulation of the ATLAS 1-lepton search does not provide a neat exclusion limit in the region $m_{\tilde{t}_1} - m_{\tilde{\chi}_1^0} < m_t$, the α_T search simulation does. It is a known issue, on the other hand, that this region is very sensitive to signals from initial state radiation, and for this reason the experimental collaborations generally tend to avoid presenting their limits in that part of the parameter space. We have checked that the limits obtained with our α_T likelihood in the region $m_{\tilde{t},\tilde{b},\tilde{g}} - m_{\tilde{\chi}_1^0} > 100 \text{ GeV}$ are not due to spurious initial state jets. Therefore, while we do not show in this study this region for the ATLAS plots, as it does not give any information, we will include the parameter space $m_{\tilde{t},\tilde{b},\tilde{g}} - m_{\tilde{\chi}_1^0} > 100 \text{ GeV}$ when showing the limits obtained with the α_T search.

The CMS 3-leptons EW production search is instead insensitive to this scenario, since $\tilde{\chi}_1^0$, $\tilde{\chi}_2^0$, and $\tilde{\chi}_1^\pm$ are Higgsino-like, and the resulting spectra are highly compressed in the EW sector.

We combine the likelihood functions from the ATLAS 1-lepton and CMS α_T searches, which are obviously statistically independent, to derive 95% C.L. bounds on the lightest stops and sbottoms in Scenario 1. They can be inferred from the boundary between the cyan diamonds and blue triangles in Fig. 3(b) and in Fig. 3(c), for the $(m_{\tilde{b}_1}, m_{\tilde{\chi}_1^0})$ and $(m_{\tilde{t}_1}, m_{\tilde{\chi}_1^0})$ planes, respectively. For comparison, the dashed black line in Fig. 3(b) gives the official 95% C.L. in SMS T2bb for the CMS α_T search, which is one of the SMS we used for validation of our procedure as described in Sec. 3.3. Equivalently, the dashed black line in Fig. 3(c) gives the official 95% C.L. in SMS TN for the ATLAS 1-lepton search.

One can see in Fig. 3(b) that, for a neutralino in the mass range $75 \text{ GeV} \leq \tilde{\chi}_1^0 \lesssim 300 \text{ GeV}$ $m_{\tilde{b}_1} \lesssim 700 \text{ GeV}$ is excluded at the 95% C.L., and in Fig. 3(c) that for $75 \text{ GeV} \leq \tilde{\chi}_1^0 \lesssim 250 \text{ GeV}$ $m_{\tilde{t}_1} \lesssim 650 \text{ GeV}$ is excluded at the 95% C.L.

Notice that the results presented in Fig. 3(b) and Fig. 3(c) are in a good agreement with Fig. 7 of Ref. [17], where the limits from five CMS and ATLAS stop/sbottom searches were combined for a model with light and almost degenerate \tilde{t}_1 , \tilde{t}_2 and \tilde{b}_1 in the spectrum. A slightly weaker bound in the case of \tilde{t}_1 comes from the fact that in our case stops and sbottoms are not degenerate, and the sbottom is in most cases heavier than the lightest stop. This also explains the presence of points excluded at 95% C.L. for $m_{\tilde{b}_1} > 1 \text{ TeV}$ in Fig. 3(b), which are characterized by \tilde{t}_1 light enough to be tested by the LHC.

In Fig. 4(a) we project the bounds to the $(m_{\tilde{Q}_3}, m_{\tilde{u}_3})$ plane, since those are, together with μ and $|A_t|$, the soft SUSY-breaking parameters that determine the fine-tuning measure, as shown in Eqs. (4) and (5). We then calculate Δ according to Eq. (1), for a conservative value $\Lambda = 10 \text{ TeV}$. The result is shown, for the same plane, in Fig. 4(b), where we only show the points that are not excluded at the 95% C.L. by the LHC.

One can see in Fig. 4(b) a handful of points characterized by $\Delta < 25$, and some more with $25 \leq \Delta < 50$. Notice, though, that we could not find any points with $\Delta < 20$. The points with $\Delta < 25$ show small stop mixing, $|A_t| \lesssim 1000 \text{ GeV}$, and they all lie in the region of the parameter space with $m_{\tilde{t}_1} \leq 800 \text{ GeV}$ and $\mu \leq 300 \text{ GeV}$. It is therefore safe to say that these points are likely to be excluded in the early stages of the LHC $\sqrt{s} = 14 \text{ TeV}$ run.

On the other hand, a much larger number of points presents $\Delta < 75$. These points are

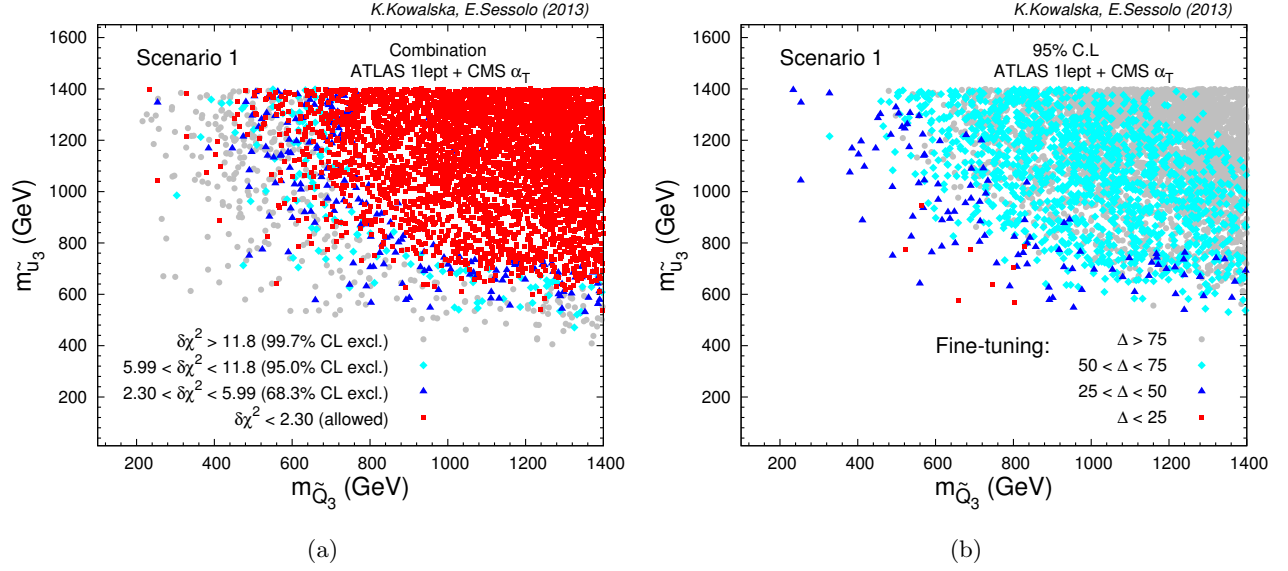


Figure 4: (a) Exclusion levels in the $(m_{\tilde{Q}_3}, m_{\tilde{u}_3})$ plane from our combination of the ATLAS 1-lepton and CMS α_T searches in Scenario 1. The color code is the same as in Fig. 1. (b) Scatter plot of the fine-tuning measure Δ in the $(m_{\tilde{Q}_3}, m_{\tilde{u}_3})$ plane for the points that are not excluded at the 95% C.L. by the LHC in Scenario 1. Red squares correspond to $\Delta < 25$, blue triangles to $25 < \Delta < 50$, cyan diamonds to $50 < \Delta < 75$, and gray dots to $\Delta > 75$.

scattered over a wider region of the parameter space and their exclusion in the near future seems more unlikely.

In Fig. 5(a), we show a scatter plot in the $(m_{\tilde{t}_1}, m_h)$ plane of the fine-tuning measure Δ for the points allowed by the LHC constraints. We consider a conservative window $m_h = 125 \pm 5$ GeV to make sure we take into account the large theoretical uncertainties associated with the calculation of the Higgs mass (we use the value of m_h given by `softsusy` in this paper), which have been estimated to be of the order of 3 GeV [4].

One can see that none of the points with the lowest fine tuning, which were shown as red squares in Fig. 4(b), have m_h consistent with the experimental value. In this sense we agree with [5, 17, 15], i.e., with the possible exclusion of the region with compressed spectra, there seem to be no room for points with small Δ given the present status of LHC searches and the measurement of the Higgs mass. Moreover, the value of m_h can be accommodated for points with $25 \leq \Delta < 50$ only with the help of a considerable theoretical error added downward to the numerical calculation.

As mentioned in Sec. 2, we find that all the points that survive the LHC and Higgs mass bounds, which are shown in Fig. 5(a), satisfy the constraints on $\text{BR}(\bar{B} \rightarrow X_s \gamma)$ and $\text{BR}(B_s \rightarrow \mu^+ \mu^-)$ at 2σ (we adopt the central values and uncertainties given in Table 2 of Ref [7]). Therefore we refrain from showing scatter plots of their distributions in this study.

The relic density constraints deserves more consideration. In Scenario 1 the lightest neu-

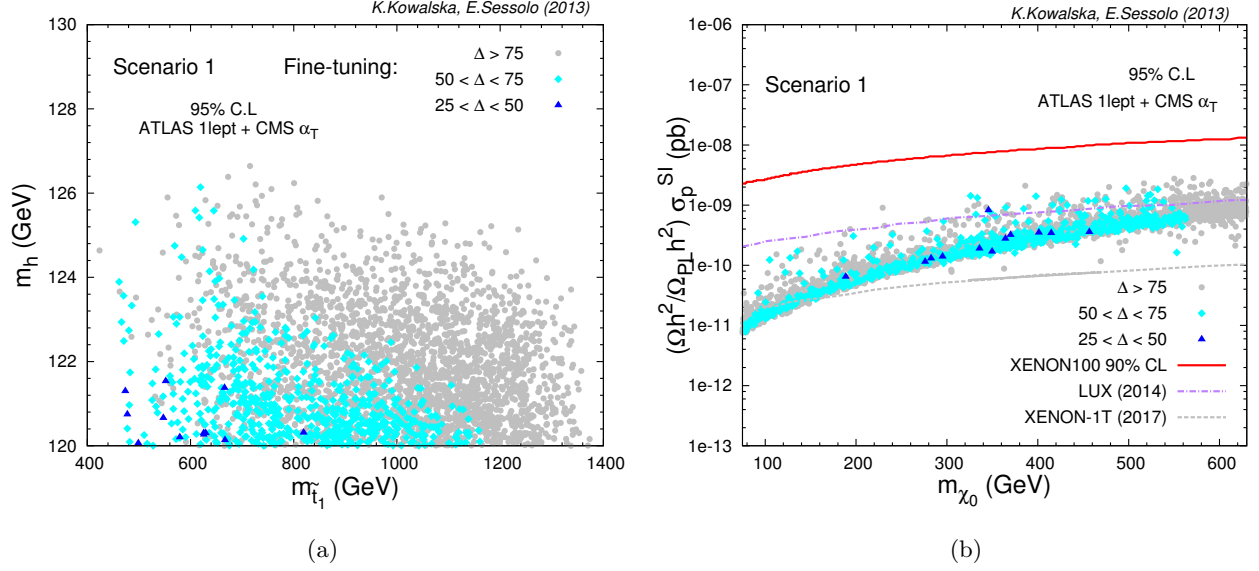


Figure 5: Scatter plot of the fine-tuning measure Δ for the points not excluded at the 95% C.L. by the LHC and characterized by $m_h \geq 120$ GeV in Scenario 1 in (a) the (m_{t1}, m_h) plane and (b) the $(m_{\chi_1^0}, \Omega_\chi h^2 / \Omega_{Pl} h^2 \cdot \sigma_p^{SI})$ plane. The solid red line shows the 90% C.L. bound from XENON100, while the dot-dashed purple and dashed gray lines show future sensitivities at LUX and XENON1T, respectively. The color code is the same as in Fig. 4(b).

tralino is Higgsino-like, and its mass is approximately equal to the value of the μ parameter. The relic density is in this case easily expressed in terms of μ , $\Omega h^2 \approx 0.1 \cdot (\mu/\text{TeV})^2$ [55]. For values in our scanned range, $75 \text{ GeV} < \mu \leq 630 \text{ GeV}$, the relic density yields for all points a value between 0.001 and 0.05. One can consider the case where the neutralino is not the sole component of dark matter, see e.g. [56]. In this case, assuming that the local density of neutralinos is obtained by the total local density by rescaling with a correction factor, $\Omega_\chi h^2 / \Omega_{Pl} h^2$, we rescale the value of the SI neutralino-proton scattering cross section and in this way account for the weakening of the signal at the underground detector. We show in Fig. 5(b) the scatter plot of the fine-tuning measure in the $(m_{\chi_1^0}, \Omega_\chi h^2 / \Omega_{Pl} h^2 \cdot \sigma_p^{SI})$ plane for the points that satisfy the Higgs mass and LHC constraints (the points of Fig. 5(a)). As expected, the value of σ_p^{SI} is independent of the level of fine tuning and the distribution of points agrees with the results of [56], in which the same calculation was performed for a natural NUHM2 type of model.

We compare our scattered points with the 90% C.L. bound from XENON100 [57] (solid red line) and we also show sensitivities at LUX [58] (dot-dashed purple line) and XENON1T [59] (dashed gray line). The latter in particular should be able to test a very significant part of the parameter space of the model.³

³The theoretical uncertainties on σ_p^{SI} due to the pion-nucleon Σ term can significantly reduce the impact of the XENON100 limit, as well as the prospects for the future sensitivities, as shown in detail in [7].

4.2 Scenario 2

In this scenario the spectra are characterized by the same set of particles as in Scenario 1, but this time the gluino can be lighter than the squarks of the third generation and within reach of the LHC. We will see that this property makes this scenario more constrained than Scenario 1. On the other hand, we do not expect variations in the overall level of fine-tuning, since already in Scenario 1 the contribution to Δ of the decoupled gluino was generally less important than the ones due to μ or the third generation squarks.

The CMS α_T search places limits on gluinos decaying to stops and sbottoms, as discussed in Sec. 3.3. On the other hand, the mass of the gluino is also strongly constrained by the ATLAS 1-lepton search, in spite of the fact that the latter was designed for detection of directly produced stops. We show in Fig. 6(a) the impact of the ATLAS search on the $(m_{\tilde{g}}, m_{\tilde{\chi}_1^0})$ plane, for which ATLAS did not provide an official exclusion bound. Neglecting the region on the left of the plot, for which the spectrum is compressed, we derive a strong bound, $m_{\tilde{g}} \gtrsim 1200$ GeV, from the ATLAS 1-lepton search in this scenario. Interestingly, this limit is in good agreement with the bound obtained in the same plane by the CMS single-lepton + b -jets + MET search [53].

We can now statistically combine the ATLAS 1-lepton and CMS α_T searches to provide a stronger bound on the $(m_{\tilde{g}}, m_{\tilde{\chi}_1^0})$ plane, which can be inferred in Fig. 6(b) from the boundary between the cyan diamonds and blue triangles. Although strongly dominated by the constraining power of the α_T search, the exclusion in Fig. 6(b) is stronger than in each individual case.

We show the exclusion plot from our statistical combination in the $(m_{\tilde{t}_1}, m_{\tilde{\chi}_1^0})$ plane in Fig. 6(c). There are many more points excluded at the 95% C.L. than in Scenario 1, due to the presence of a light gluino in the spectrum. This makes it more difficult to find points with $m_{\tilde{t}_1} \lesssim 650$ GeV than in Scenario 1.

We summarize the LHC limits for Scenario 2 in Fig. 6(d) where we show the exclusion plot in the $(m_{\tilde{g}}, m_{\tilde{t}_1})$ plane. Most points with $m_{\tilde{g}} \leq 1200$ GeV are excluded independently of the value of the stop mass. The points that are not excluded in the region $m_{\tilde{g}} \simeq 800$ GeV are the ones close to the compressed spectra region for the gluinos, shown on the top left in Fig. 6(b). The points in the range $400 \text{ GeV} \lesssim m_{\tilde{t}_1} \lesssim 600 \text{ GeV}$ that are not excluded at the 95% C.L. (gray points and cyan diamonds) are the points close to the compressed spectra region for the stops, shown in Fig. 6(c) in the range $300 \text{ GeV} \lesssim m_{\tilde{\chi}_1^0} \lesssim 400 \text{ GeV}$.

The limits do not change by including the CMS 3-lepton EW production search as, similarly to Scenario 1, the neutralino is Higgsino-like and the 3-lepton search is not sensitive to spectra compressed in the EW sector.

In Fig. 7(a) we show the distribution of the fine-tuning measure Δ in the $(m_{\tilde{g}}, m_{\tilde{t}_1})$ plane, for the points allowed by the LHC searches at the 95% C.L. We remind the reader that we use $\Lambda = 10$ TeV. One can see that the region with $m_{\tilde{g}} \simeq 800$ GeV presents a large degree of fine-tuning, as could be expected since $\mu \simeq 600$ GeV for these points. As was the case in Scenario 1, the points with the lowest fine-tuning, $\Delta < 50$, are characterized by stops masses not exceeding 800 GeV, independently of the other parameters. Differently from Scenario 1, however, we could not find any points with $\Delta < 25$, a fact that appears clear by comparing Fig. 7(b) with Fig. 4(b),

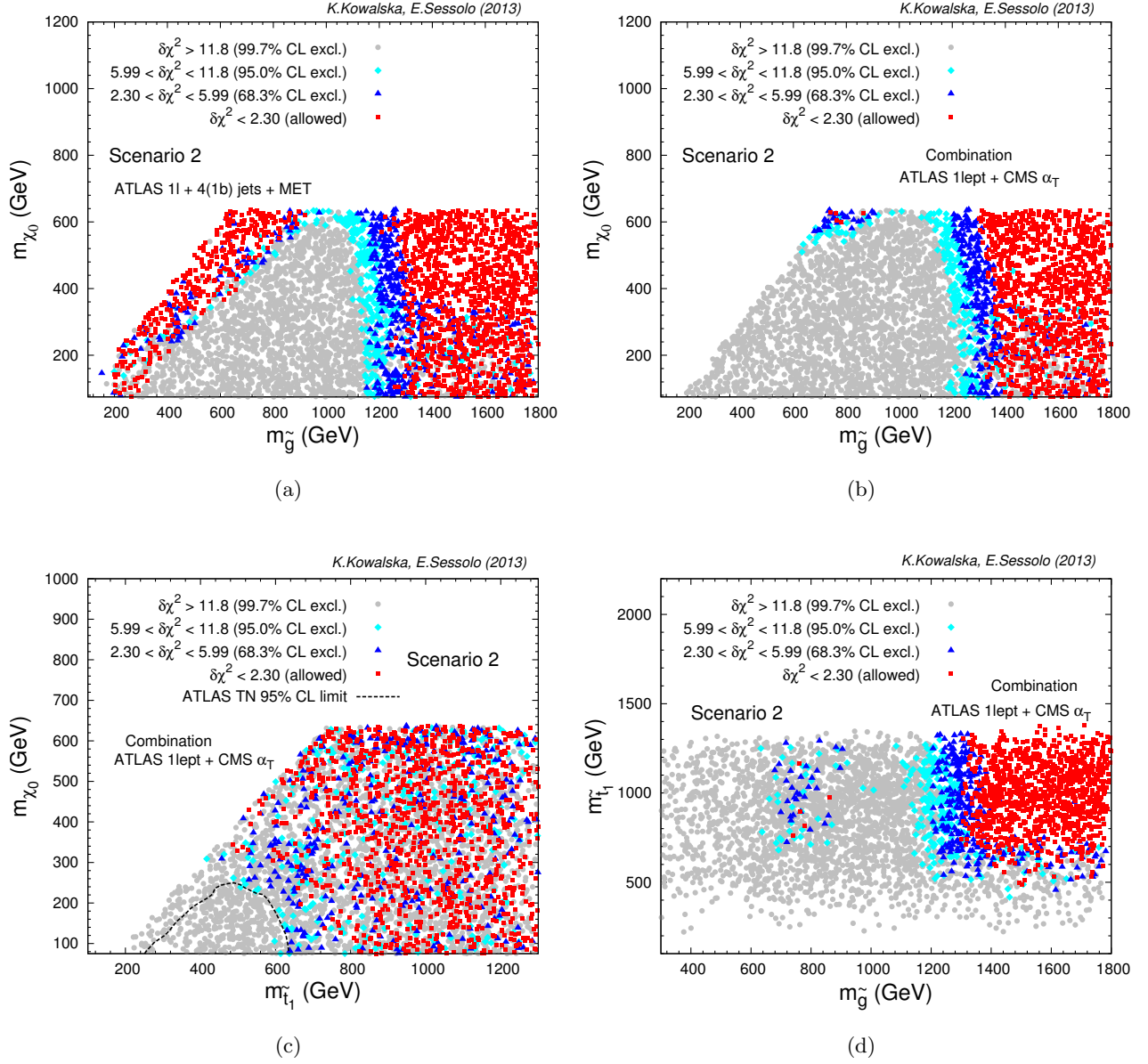


Figure 6: Exclusion levels in the $(m_{\tilde{g}}, m_{\tilde{\chi}_1^0})$ plane from (a) our simulation of the ATLAS 1-lepton search and (b) our combination of the ATLAS 1-lepton and CMS α_T searches in Scenario 2. Exclusion levels from the same combination in (c) the $(m_{\tilde{t}_1}, m_{\tilde{\chi}_1^0})$ plane and (d) the $(m_{\tilde{g}}, m_{\tilde{t}_1})$ plane. The color code is the same as in Fig. 1.

where the distribution of Δ for the points allowed by the LHC is shown in the $(m_{\tilde{Q}_3}, m_{\tilde{u}_3})$ plane for Scenarios 2 and 1, respectively. As mentioned above, the reason is that Scenario 2 is more constrained than Scenario 1 because of the light gluinos in the spectra. Thus, points with low fine-tuning, which were rare in the framework of Scenario 1, become even more difficult to find in Scenario 2.

Finally, Scenario 2, does not show relevant differences with respect to Scenario 1 when it

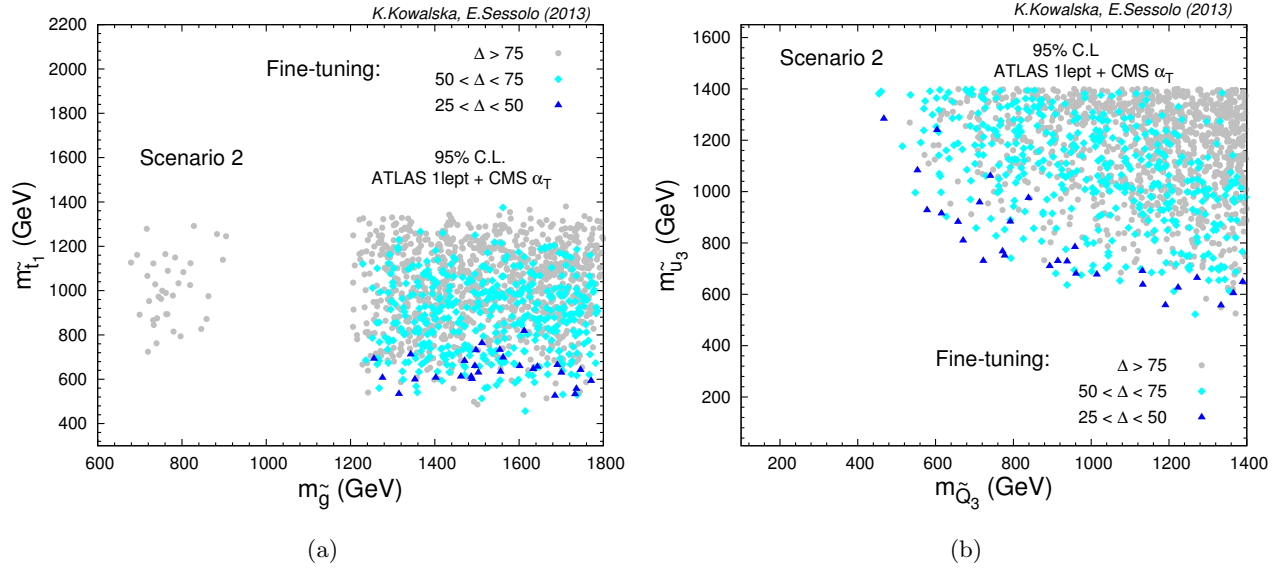


Figure 7: Scatter plot of the fine-tuning measure Δ for the points that are not excluded at the 95% C.L. by the LHC in Scenario 2 for (a) the $(m_{\tilde{g}}, m_{\tilde{t}_1})$ plane and (b) the $(m_{\tilde{Q}_3}, m_{\tilde{u}_3})$ plane. The color code is the same as in Fig. 4(b).

comes to the other phenomenological observables, since their value in the MSSM does not depend strongly on the gluino mass. We found less points than in Scenario 1 having $\Delta < 50$ and being consistent with the Higgs mass measurement. However, the distribution on the $(m_{\tilde{t}_1}, m_h)$ plane does not look significantly different from Fig. 5(a), and we refrain from showing it over here.

The bounds from $\text{BR}(B_s \rightarrow \mu^+ \mu^-)$ and $\text{BR}(\bar{B} \rightarrow X_s \gamma)$ are satisfied at 2σ for the parameter space allowed by the LHC, and the relic density assumes the same values as in Scenario 1 when μ is taken equal. Consequently, the prospects for direct detection searches do not change with respect to Scenario 1.

4.3 Scenario 3

We analyze the impact of our selected LHC searches in a more complex scenario, whose spectra are characterized by the presence of light sleptons of the three generations, a bino-like lightest neutralino, $\tilde{\chi}_1^0$, and wino-like $\tilde{\chi}_2^0$ and $\tilde{\chi}_1^\pm$, in addition to the particles of Scenario 2. We point out here that the level of fine-tuning in this scenario is higher than in the previous ones, $\Delta_\mu \simeq 100$ in Scenario 3, since the μ parameter is fixed, $\mu = 630$ GeV. We will, nonetheless, calculate the fine-tuning measure due to the other soft SUSY-breaking parameters, hereafter indicated with $\bar{\Delta}$, to describe the impact of the contributions from the squark and gluino sectors.

This scenario presents some novel features. First, it allows investigation of the EW sector of the theory with the CMS 3-lepton + MET search, since the gaugino nature of $\tilde{\chi}_1^0$, $\tilde{\chi}_2^0$ and $\tilde{\chi}_1^\pm$ leads to hierarchical spectra that can produce hard leptons in the decay chain. Second, it allows

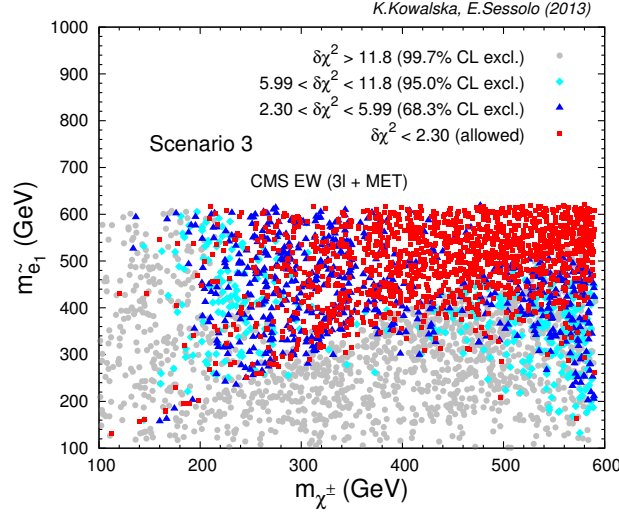


Figure 8: Exclusion levels in the $(m_{\tilde{\chi}_1^\pm}, m_{\tilde{e}_1})$ plane from our simulation of the CMS 3-lepton EW production search in Scenario 3. The color code is the same as in Fig. 1.

to investigate the impact of the ATLAS 1-lepton and CMS α_T searches on spectra significantly more complex than the ones associated with generic SMS. Thus, the exclusion bounds on gluinos and third generation squarks might be altered with respect to Scenarios 1 and 2. Third, the gaugino nature of the neutralino leads to different dark matter signatures.

We do not consider in this paper the case of a wino-like neutralino, $\tilde{\chi}_1^0 \approx \tilde{\chi}_1^\pm$ ($M_2 < M_1$), as in that case the decay chain $\tilde{\chi}_1^\pm \rightarrow \tilde{\chi}_1^0$ yields the same experimental features as in the Higgsino case, i.e. the decay products are soft and the efficiencies are very small. On the other hand, the cross section for production of $\tilde{\chi}_2^0 \tilde{\chi}_1^0$ and $\tilde{\chi}_2^0 \tilde{\chi}_1^\pm$ pairs, where the heavier particle is boosted, would be highly suppressed: the former by the fact that the Higgsino component of both produced particles is close to zero; the latter by vanishing elements of the neutralino mixing matrix. Thus, in the wino neutralino case the impact of the EW sector on the bounds on the gluino and stop/sbottom masses would be negligible.

The CMS EW 3-lepton search is not sensitive to production of stops/sbottoms or gluinos, which yield hadronic final states with jets. In Scenario 3, it can thus only constrain $\tilde{\chi}_1^+ \tilde{\chi}_1^-$ and $\tilde{\chi}_1^\pm \tilde{\chi}_2^0$ pair production. For each model point the impact of this search depends strongly on whether a slepton with mass between the masses of $\tilde{\chi}_1^\pm$ ($\tilde{\chi}_2^0$) and $\tilde{\chi}_1^0$ is present in the spectrum. Thus a scatter plot in the $(m_{\tilde{\chi}_1^\pm}, m_{\tilde{\chi}_1^0})$ plane will look less informative than in the case of the SMS that we simulated for validation and comparison with the experimental result, shown in Fig. 1(b). It is instead more istructive to look at the exclusion plot in the $(m_{\tilde{\chi}_1^\pm}, m_{\tilde{e}_1})$ plane, which we show in Fig. 8. One can identify two regions excluded at the 95% C.L.: one at $m_{\tilde{\chi}_1^\pm} < 200$ GeV, irrespectively of the slepton mass, where the three-body decays $\tilde{\chi}_1^\pm \rightarrow \nu_l l^\pm \tilde{\chi}_1^0$ and $\tilde{\chi}_2^0 \rightarrow l^+ l^- \tilde{\chi}_1^0$ are mediated by off-shell sleptons, and one at $m_{\tilde{\chi}_1^\pm} > m_{\tilde{e}_1}$, which extends to $m_{\tilde{\chi}_1^\pm} \simeq 500 - 600$ GeV, where the effects of on-shell sleptons enhance the signal and increase

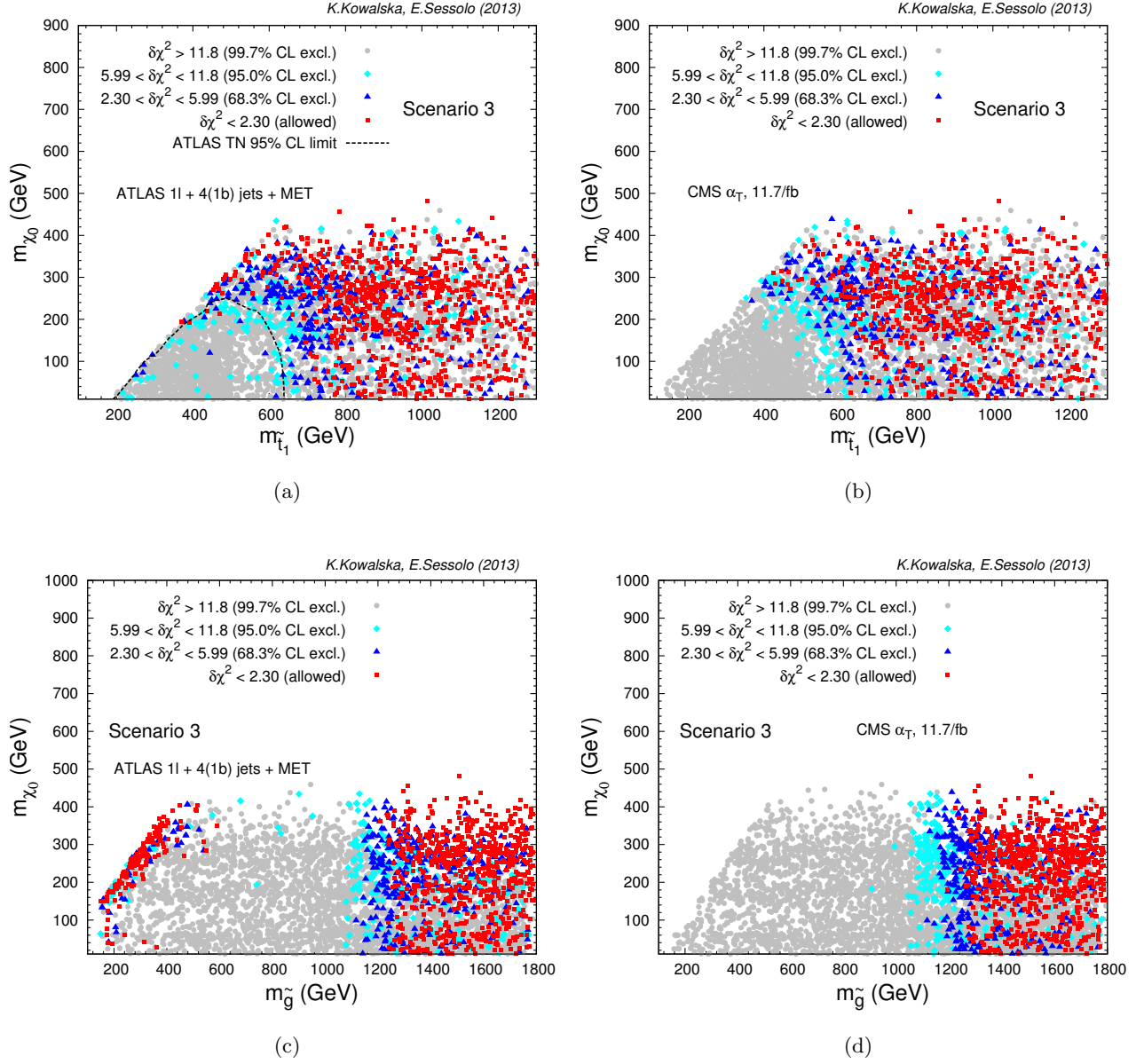


Figure 9: Exclusion levels in the $(m_{\tilde{t}_1}, m_{\tilde{\chi}_1^0})$ plane from our simulation of (a) the ATLAS 1-lepton search and (b) the CMS α_T search in Scenario 3. The dashed black line shows the published ATLAS 95% C.L. bound in SMS TN. Exclusion levels in the $(m_{\tilde{g}}, m_{\tilde{\chi}_1^0})$ plane from our simulation of (c) the ATLAS 1-lepton search and (d) the CMS α_T search in Scenario 3. The color code is the same as in Fig. 1.

the sensitivity. The sensitivity drops with increasing chargino masses, faster for the first region since the decay products are softer. One can also see that in the case of on-shell intermediate sleptons the sensitivity bound depends strongly on the slepton mass, reaching its maximum when $m_{\tilde{e}_1} \approx 0.5m_{\tilde{\chi}_1^\pm} + 0.5m_{\tilde{\chi}_1^0}$, which is the case of the SMS shown in Fig. 1(b).

As will appear clear below, for complex spectra it becomes very important to combine

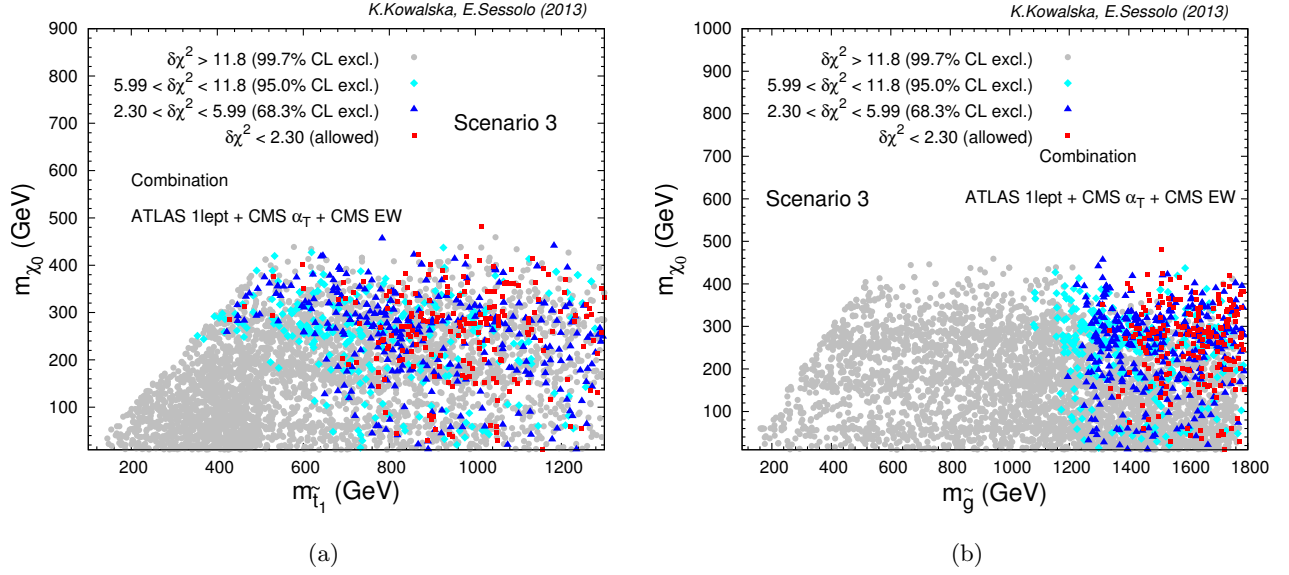


Figure 10: Exclusion levels from our combination of the ATLAS 1-lepton, CMS α_T , and CMS EW production searches in (a) the $(m_{\tilde{t}_1}, m_{\tilde{\chi}_1^0})$ plane and (b) the $(m_{\tilde{g}}, m_{\tilde{\chi}_1^0})$ plane in Scenario 3. The color code is the same as in Fig. 1.

independent searches that investigate different topologies. This is because, as was mentioned in Sec. 1, the bounds on SUSY masses from an individual search can in some cases be weakened with respect to the ones obtained in the framework of a SMS. To give a practical example, we show in Fig. 9(a) the exclusion plot in the $(m_{\tilde{t}_1}, m_{\tilde{\chi}_1^0})$ plane for the ATLAS 1-lepton search in Scenario 3. One can see that, as was the case for Scenario 2, many points with $m_{\tilde{t}_1} \gg 800$ GeV are excluded due to the presence of a light gluino in the spectra. On the other hand, there are some points not excluded at the 95% C.L., or at the 99.7% C.L., in the region of the parameter space that was strongly excluded in SMS TN. Some caution is required when trying to draw definite conclusions about these points, since their number is not large. Moreover, we repeat that our criterion for exclusion is just an approximation, and carries with it some limitations. However, taking the exclusion C.L. at face value, we gave a closer look at the PYTHIA event distribution of these points, finding that they are characterized by a large number of events with no hard isolated lepton in the final state, which give no signal, or by events that involve taus in the final state, for which reconstruction is a delicate task. A typical decay chain is, for example, $\tilde{t} \rightarrow \tilde{b}\tilde{\chi}_1^\pm$, where the chargino decays through intermediate $\tilde{\tau}$ or $\tilde{\nu}_\tau$, $\tilde{\chi}_1^\pm \rightarrow \tau^\pm \nu_\tau \tilde{\chi}_1^0$, and the τ decays hadronically. It is also not trivial to investigate the effects that these events have on the overall efficiencies, given the large number of kinematical boxes we employ in our simulation. But, in any case, one can see in Fig. 9(b) that the α_T search produces a more stable exclusion line in the $(m_{\tilde{t}_1}, m_{\tilde{\chi}_1^0})$, due to the statistical combination of different final state topologies.

We show for comparison the exclusion plots in the $(m_{\tilde{g}}, m_{\tilde{\chi}_1^0})$ for the ATLAS 1-lepton and CMS α_T searches in Figs 9(c) and 9(d), respectively.

In Fig. 10(a) we show the statistical combination of the ATLAS 1-lepton, CMS α_T , and CMS EW production searches in the $(m_{\tilde{t}_1}, m_{\tilde{\chi}_1^0})$ plane. In Fig. 10(b) we show the same, in the $(m_{\tilde{g}}, m_{\tilde{\chi}_1^0})$ plane. One can see that the combination of all our searches strongly reduces the number of allowed points in Scenario 3. With the exception of a few points for which the spectra show features similar to the SMS, i.e. $m_{\tilde{t}_1} \ll m_{\tilde{g}}$ and $\tilde{\chi}_1^\pm$ or sleptons too heavy to produce a signature in the 3-lepton search (points that become increasingly rare to find in the plots), Fig. 10 shows that stops are bound to $m_{\tilde{t}_1} \gtrsim 700$ GeV for a light $\tilde{\chi}_1^0$, while the bound on the gluino mass does not change significantly from Scenario 2.

Thus we can see that, in spite of the limitations that might emerge with complex spectra in an individual search, a statistical combination of different and possibly independent searches, from both ATLAS and CMS for instance, stabilizes the bounds and strongly reduces the allowed regions of the parameter space, thus producing limits on the individual masses that are enhanced with respect to the case of selected SMS. Given the nature of certain decay chains observed in Scenario 3, we suspect that even stronger constraints might be obtained by including additional mixed searches, e.g. EW production with taus that decay hadronically in the final state [60].

Similar conclusions were already drawn in [16] for a combination of CMS searches at $\sqrt{s} = 7$ TeV, in an original presentation style that involved “traffic light” plots. We confirm this result over here, where we limit ourselves to presenting the likelihood-based C.L. exclusion levels for the points generated in our scenarios.

We show in Fig. 11(a) the distribution of the fine-tuning measure $\bar{\Delta}$ in the $(m_{\tilde{g}}, m_{\tilde{t}_1})$ plane for the points allowed by the LHC at the 95% C.L. We neglect the contribution due to μ , $\Delta_\mu \simeq 100$, as explained at the beginning of this subsection.

When neglecting μ , the distribution of $\bar{\Delta}$ in Scenario 3 shows overall lower values than the equivalent distribution for Δ in Scenario 2. Several points with $m_{\tilde{t}_1} < 800$ GeV, which were characterized by $25 < \Delta < 50$ in Scenario 2, now show $\bar{\Delta} < 25$, even if Scenario 3 is much more constrained by the LHC than Scenario 2. Thus, it appears to us that the greatest obstacle to obtaining MSSM spectra with an acceptable level of EW fine-tuning after the LHC comes from the difficulty of finding regions of the parameter space characterized by small enough values of the parameter μ . In this sense, neglecting the pockets of the parameter space that give compressed spectra, at the moment the LHC limits on μ are more constraining for naturalness than the limits on the third generation squarks.

Clearly, inclusion of the Higgs mass constraint makes the above conclusion less relevant. In fact, again none of the points shown as red squares in Fig. 11(a) presents $m_h > 120$ GeV.

Finally, in Scenario 3 the relic density shows a larger range of values than in Scenarios 1 and 2. On the other hand, in general bino-like neutralino dark matter tends to overclose the Universe, unless the $\tilde{\chi}_1^0 \tilde{\chi}_1^0$ annihilation rate is boosted by one of the known mechanism for obtaining the correct relic density in the MSSM, see, e.g., [7]. As a matter of fact, after including the constraints from the LHC, the Higgs mass, $\text{BR}(B_s \rightarrow \mu^+ \mu^-)$, $\text{BR}(\bar{B} \rightarrow X_s \gamma)$, and a 2σ upper bound for the relic density, we found that only 76 points survived in our Scenario 3.

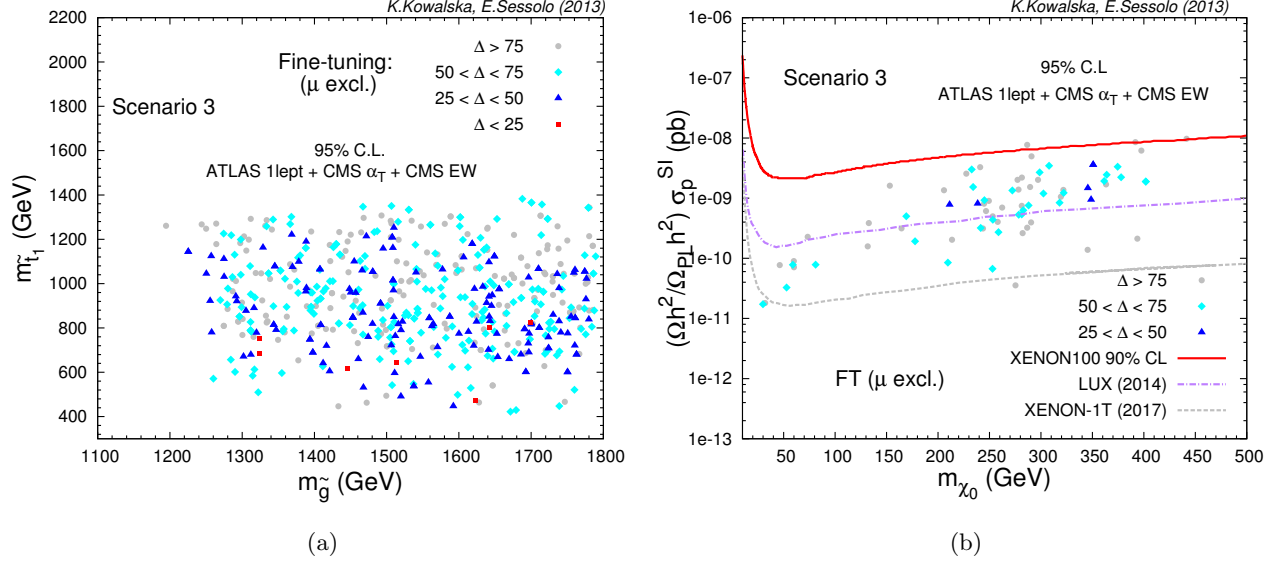


Figure 11: (a) Scatter plot of the fine-tuning measure $\bar{\Delta}$ in the $(m_{\tilde{g}}, m_{\tilde{t}_1})$ plane for the points that are not excluded at the 95% C.L. by the LHC in Scenario 3. (b) Scatter plot of $\bar{\Delta}$ in the $(m_{\tilde{\chi}_1^0}, \Omega_{\tilde{\chi}} h^2 / \Omega_{\text{Planck}} h^2 \cdot \sigma_p^{\text{SI}})$ plane for the points not excluded at the 95% C.L. by the LHC, with $m_h \geq 120$ GeV and the constraints from the relic density (upper limit), $\text{BR}(\text{B}_s \rightarrow \mu^+ \mu^-)$, and $\text{BR}(\bar{\text{B}} \rightarrow \text{X}_s \gamma)$ satisfied at 2σ in Scenario 3. The solid red line shows the 90% C.L. bound from XENON100, while the dot-dashed purple and dashed gray lines show future sensitivities at LUX and XENON1T, respectively. The color code is the same as in Fig. 4(b).

We show a scatter plot of their $\bar{\Delta}$ in the $(m_{\tilde{\chi}_1^0}, \Omega_{\tilde{\chi}} h^2 / \Omega_{\text{Planck}} h^2 \cdot \sigma_p^{\text{SI}})$ plane in Fig. 11(b), where we also show the 90% C.L. exclusion bound by XENON100 and the sensitivities at LUX and XENON1T.

5 Summary

In this paper we investigated the impact of three different LHC direct SUSY searches on the parameter space of the MSSM on which we imposed a loose requirement of naturalness, $\Delta^{-1} > 1\%$ with $\Lambda = 10$ TeV.

We considered three different scenarios. In Scenario 1 the SUSY spectra consist of light stops, sbottoms and Higgsino-like lightest chargino and neutralino, while the other sparticles are out of reach at the LHC; in Scenario 2 we considered the presence of an additional light gluino in the spectra; and in Scenario 3 we considered a more complex kind of spectrum, characterized by light stops, sbottoms, gluinos, sleptons of the three generations, a bino-like lightest neutralino and wino-like lightest chargino. By construction, Scenario 3 is always more fine-tuned than Scenarios 1 and 2.

For each generated point in our scenarios we performed detailed on-the-fly simulation of the following LHC searches based on the $\sqrt{s} = 8$ TeV data-set: the 21/fb ATLAS direct stop

production search with 1 lepton in the final state, the 9.2/fb CMS 3-lepton EW production search, and the 11.7/fb CMS α_T inclusive search for squarks and gluinos. For each point we calculated the exclusion C.L. due to the individual searches and to their statistical combination. We then calculated the level of fine-tuning and some relevant phenomenological observables: the Higgs mass, the relic density of dark matter, $\text{BR}(\text{B}_s \rightarrow \mu^+ \mu^-)$, $\text{BR}(\bar{\text{B}} \rightarrow \text{X}_s \gamma)$, and the neutralino-proton SI cross-section, σ_p^{SI} .

We showed that, when considering increasingly complex spectra with respect to the simplified models for which the experimental collaborations provide official limits on the sparticle masses, and at the same time combining different searches, two competing effects can emerge. On the one hand, a more complex spectra involves longer decay chains than a SMS, which can in some occasions produce topologies to which an individual search is not sensitive and thus reduce the signal strength. On the other hand, a combination of different searches strongly limits the available parameter space for complex, well separated spectra, thus overcoming the above limitations and placing strong bounds on certain scenarios.

To give an example from our discussion, consider the region with $m_{\tilde{\chi}_1^0} \lesssim 250 \text{ GeV}$ in Scenario 3. While it is not possible to say that stops with $600 \text{ GeV} \lesssim m_{\tilde{t}_1} \lesssim 700 \text{ GeV}$ are absolutely excluded by any one of our implemented searches, it is certainly more unlikely than in, say, Scenario 1 to find a point for which the stop mass falls in the above range and, at the same time, either gluinos, or $\tilde{\chi}_1^\pm$ and $\tilde{\chi}_2^0$ are not excluded by the remaining searches. We thus appreciate the effort of the experimental collaborations in providing a great number of limits obtained with different topologies, and encourage them to produce statistical combination of independent results, even combining the ATLAS and CMS data sets.

As pertains to the naturalness of the scenarios considered here we showed that, if one neglects compressed spectra, which we did not treat in this study, the present LHC limits on the squarks of the third generation and, more importantly, the μ parameter exclude points with $\Delta < 20$. Only a handful of points in Scenario 1, characterized by $\mu < 300 \text{ GeV}$, $m_{\tilde{t}_1} \lesssim 800 \text{ GeV}$, and $|A_t| \lesssim 1000 \text{ GeV}$ were found with $\Delta < 25$, and they all presented a Higgs mass well below the experimental value, even if one considers a large theoretical uncertainty in the Higgs mass calculation. The constraints from $\text{BR}(\text{B}_s \rightarrow \mu^+ \mu^-)$ and $\text{BR}(\bar{\text{B}} \rightarrow \text{X}_s \gamma)$ can instead be satisfied more easily for the parameter space presently allowed by the LHC.

As is well known, finally, for Higgsino dark matter the relic density tends to be too low with respect to the value measured by PLANCK and WMAP. For bino-dark matter it tends instead to overclose the Universe, unless the annihilation cross section is enhanced through coannihilation or resonance effects, which have been largely explored in the literature. Nonetheless, we showed that the three scenarios considered here lie in the area of interest of direct detection experiments, even when rescaling their possible signal. We presented the prospects for future observation of dark matter in these scenarios at the underground experiments LUX and XENON1T.

ACKNOWLEDGMENTS

We would like to thank Maurizio Pierini for a useful e-mail exchange on the implementation

of signal efficiencies. We would also like to thank Leszek Roszkowski, Yue-Lin Sming Tsai, and Shoaib Munir for many discussions. We are funded in part by the Welcome Programme of the Foundation for Polish Science. K.K. is supported by the EU and MSHE Grant No. POIG.02.03.00-00-013/09. The use of the CIS computer cluster at NCBJ is gratefully acknowledged.

References

- [1] **CMS** Collaboration, S. Chatrchyan *et al.*, “Observation of a new boson at a mass of 125 GeV with the CMS experiment at the LHC,” *Phys.Lett.* **B716** (2012) 30–61, [arXiv:1207.7235 \[hep-ex\]](#).
- [2] **ATLAS** Collaboration, G. Aad *et al.*, “Observation of a new particle in the search for the Standard Model Higgs boson with the ATLAS detector at the LHC,” *Phys.Lett.* **B716** (2012) 1–29, [arXiv:1207.7214 \[hep-ex\]](#).
- [3] **LHCb** Collaboration, R. Aaij *et al.*, “First evidence for the decay $B_s \rightarrow \mu^+ \mu^-$,” *Phys.Rev.Lett.* **110** (2013) 021801, [arXiv:1211.2674 \[hep-ex\]](#).
- [4] S. Heinemeyer, O. Stal, and G. Weiglein, “Interpreting the LHC Higgs Search Results in the MSSM,” *Phys.Lett.* **B710** (2012) 201–206, [arXiv:1112.3026 \[hep-ph\]](#).
- [5] L. J. Hall, D. Pinner, and J. T. Ruderman, “A Natural SUSY Higgs Near 126 GeV,” *JHEP* **1204** (2012) 131, [arXiv:1112.2703 \[hep-ph\]](#).
- [6] H. Baer, V. Barger, and A. Mustafayev, “Implications of a 125 GeV Higgs scalar for LHC SUSY and neutralino dark matter searches,” *Phys.Rev.* **D85** (2012) 075010, [arXiv:1112.3017 \[hep-ph\]](#). ; A. Arbey *et al.*, “Implications of a 125 GeV Higgs for supersymmetric models,” *Phys.Lett.* **B708** (2012) 162–169, [arXiv:1112.3028 \[hep-ph\]](#). ; M. Carena, S. Gori, N. R. Shah, and C. E. Wagner, “A 125 GeV SM-like Higgs in the MSSM and the $\gamma\gamma$ rate,” *JHEP* **1203** (2012) 014, [arXiv:1112.3336 \[hep-ph\]](#). ; J. Cao *et al.*, “A SM-like Higgs near 125 GeV in low energy SUSY: a comparative study for MSSM and NMSSM,” *JHEP* **1203** (2012) 086, [arXiv:1202.5821 \[hep-ph\]](#). ; N. D. Christensen, T. Han, and S. Su, “MSSM Higgs Bosons at The LHC,” *Phys.Rev.* **D85** (2012) 115018, [arXiv:1203.3207 \[hep-ph\]](#). ; F. Brummer, S. Kraml, and S. Kulkarni, “Anatomy of maximal stop mixing in the MSSM,” *JHEP* **1208** (2012) 089, [arXiv:1204.5977 \[hep-ph\]](#). ; A. Arbey, M. Battaglia, A. Djouadi, and F. Mahmoudi, “The Higgs sector of the phenomenological MSSM in the light of the Higgs boson discovery,” *JHEP* **1209** (2012) 107, [arXiv:1207.1348 \[hep-ph\]](#).
- [7] A. Fowlie, K. Kowalska, L. Roszkowski, E. M. Sessolo, and Y.-L. S. Tsai, “Dark matter and collider signatures of the MSSM,” [arXiv:1306.1567 \[hep-ph\]](#).
- [8] J. R. Ellis, K. Enqvist, D. V. Nanopoulos, and F. Zwirner, “Observables in Low-Energy Superstring Models,” *Mod.Phys.Lett.* **A1** (1986) 57. ; R. Barbieri and G. Giudice, “Upper Bounds on Supersymmetric Particle Masses,” *Nucl.Phys.* **B306** (1988) 63.

- [9] G. G. Ross and R. Roberts, “Minimal supersymmetric unification predictions,” *Nucl.Phys.* **B377** (1992) 571–592. ; B. de Carlos and J. Casas, “One loop analysis of the electroweak breaking in supersymmetric models and the fine tuning problem,” *Phys.Lett.* **B309** (1993) 320–328, [arXiv:hep-ph/9303291 \[hep-ph\]](#). ; G. W. Anderson and D. J. Castano, “Measures of fine tuning,” *Phys.Lett.* **B347** (1995) 300–308, [arXiv:hep-ph/9409419 \[hep-ph\]](#). ; G. W. Anderson and D. J. Castano, “Naturalness and superpartner masses or when to give up on weak scale supersymmetry,” *Phys.Rev.* **D52** (1995) 1693–1700, [arXiv:hep-ph/9412322 \[hep-ph\]](#). ; S. Dimopoulos and G. Giudice, “Naturalness constraints in supersymmetric theories with nonuniversal soft terms,” *Phys.Lett.* **B357** (1995) 573–578, [arXiv:hep-ph/9507282 \[hep-ph\]](#). ; P. Ciafaloni and A. Strumia, “Naturalness upper bounds on gauge mediated soft terms,” *Nucl.Phys.* **B494** (1997) 41–53, [arXiv:hep-ph/9611204 \[hep-ph\]](#). ; G. Bhattacharyya and A. Romanino, “Naturalness constraints on gauge mediated supersymmetry breaking models,” *Phys.Rev.* **D55** (1997) 7015–7019, [arXiv:hep-ph/9611243 \[hep-ph\]](#). ; P. H. Chankowski, J. R. Ellis, and S. Pokorski, “The Fine tuning price of LEP,” *Phys.Lett.* **B423** (1998) 327–336, [arXiv:hep-ph/9712234 \[hep-ph\]](#). ; K. L. Chan, U. Chattopadhyay, and P. Nath, “Naturalness, weak scale supersymmetry and the prospect for the observation of supersymmetry at the Tevatron and at the CERN LHC,” *Phys.Rev.* **D58** (1998) 096004, [arXiv:hep-ph/9710473 \[hep-ph\]](#). ; R. Barbieri and A. Strumia, “About the fine tuning price of LEP,” *Phys.Lett.* **B433** (1998) 63–66, [arXiv:hep-ph/9801353 \[hep-ph\]](#). ; D. Wright, “Naturally nonminimal supersymmetry,” [arXiv:hep-ph/9801449 \[hep-ph\]](#). ; P. H. Chankowski, J. R. Ellis, M. Olechowski, and S. Pokorski, “Haggling over the fine tuning price of LEP,” *Nucl.Phys.* **B544** (1999) 39–63, [arXiv:hep-ph/9808275 \[hep-ph\]](#). ; G. L. Kane and S. King, “Naturalness implications of LEP results,” *Phys.Lett.* **B451** (1999) 113–122, [arXiv:hep-ph/9810374 \[hep-ph\]](#). ; L. Giusti, A. Romanino, and A. Strumia, “Natural ranges of supersymmetric signals,” *Nucl.Phys.* **B550** (1999) 3–31, [arXiv:hep-ph/9811386 \[hep-ph\]](#). ; J. L. Feng, K. T. Matchev, and T. Moroi, “Focus points and naturalness in supersymmetry,” *Phys.Rev.* **D61** (2000) 075005, [arXiv:hep-ph/9909334 \[hep-ph\]](#). ; R. Kitano and Y. Nomura, “A Solution to the supersymmetric fine-tuning problem within the MSSM,” *Phys.Lett.* **B631** (2005) 58–67, [arXiv:hep-ph/0509039 \[hep-ph\]](#). ; D. Horton and G. Ross, “Naturalness and Focus Points with Non-Universal Gaugino Masses,” *Nucl.Phys.* **B830** (2010) 221–247, [arXiv:0908.0857 \[hep-ph\]](#). ; P. Lodone, “Naturalness bounds in extensions of the MSSM without a light Higgs boson,” *JHEP* **1005** (2010) 068, [arXiv:1004.1271 \[hep-ph\]](#).
- [10] M. Papucci, J. T. Ruderman, and A. Weiler, “Natural SUSY Endures,” *JHEP* **1209** (2012) 035, [arXiv:1110.6926 \[hep-ph\]](#).
- [11] H. Baer, V. Barger, P. Huang, D. Mickelson, A. Mustafayev, *et al.*, “Post-LHC7 fine-tuning in the mSUGRA/CMSSM model with a 125 GeV Higgs boson,” [arXiv:1210.3019 \[hep-ph\]](#).
- [12] M. Bastero-Gil, C. Hugonie, S. King, D. Roy, and S. Vempati, “Does LEP prefer the

- NMSSM?," *Phys.Lett.* **B489** (2000) 359–366, [arXiv:hep-ph/0006198 \[hep-ph\]](#). ; A. Delgado, C. Kolda, J. P. Olson, and A. de la Puente, "Solving the Little Hierarchy Problem with a Singlet and Explicit μ Terms," *Phys.Rev.Lett.* **105** (2010) 091802, [arXiv:1005.1282 \[hep-ph\]](#). ; U. Ellwanger, G. Espitalier-Noel, and C. Hugonie, "Naturalness and Fine Tuning in the NMSSM: Implications of Early LHC Results," *JHEP* **1109** (2011) 105, [arXiv:1107.2472 \[hep-ph\]](#). ; G. G. Ross and K. Schmidt-Hoberg, "The Fine-Tuning of the Generalised NMSSM," *Nucl.Phys.* **B862** (2012) 710–719, [arXiv:1108.1284 \[hep-ph\]](#).
- [13] K. Cheung, C.-W. Chiang, and J. Song, "A Minimal supersymmetric scenario with only mu at the weak scale," *JHEP* **0604** (2006) 047, [arXiv:hep-ph/0512192 \[hep-ph\]](#). ; H. Baer, V. Barger, and P. Huang, "Hidden SUSY at the LHC: the light higgsino-world scenario and the role of a lepton collider," *JHEP* **1111** (2011) 031, [arXiv:1107.5581 \[hep-ph\]](#).
- [14] R. Kitano and Y. Nomura, "Supersymmetry, naturalness, and signatures at the LHC," *Phys.Rev.* **D73** (2006) 095004, [arXiv:hep-ph/0602096 \[hep-ph\]](#). ; M. Asano, H. D. Kim, R. Kitano, and Y. Shimizu, "Natural Supersymmetry at the LHC," *JHEP* **1012** (2010) 019, [arXiv:1010.0692 \[hep-ph\]](#). ; S. Cassel, D. Ghilencea, S. Kraml, A. Lessa, and G. Ross, "Fine-tuning implications for complementary dark matter and LHC SUSY searches," *JHEP* **1105** (2011) 120, [arXiv:1101.4664 \[hep-ph\]](#). ; K. Sakurai and K. Takayama, "Constraint from recent ATLAS results to non-universal sfermion mass models and naturalness," *JHEP* **1112** (2011) 063, [arXiv:1106.3794 \[hep-ph\]](#). ; M. Perelstein and B. Shakya, "Fine-Tuning Implications of Direct Dark Matter Searches in the MSSM," *JHEP* **1110** (2011) 142, [arXiv:1107.5048 \[hep-ph\]](#). ; C. Brust, A. Katz, S. Lawrence, and R. Sundrum, "SUSY, the Third Generation and the LHC," *JHEP* **1203** (2012) 103, [arXiv:1110.6670 \[hep-ph\]](#). ; H. Baer, V. Barger, P. Huang, and X. Tata, "Natural Supersymmetry: LHC, dark matter and ILC searches," *JHEP* **1205** (2012) 109, [arXiv:1203.5539 \[hep-ph\]](#). ; H. Baer, V. Barger, P. Huang, A. Mustafayev, and X. Tata, "Radiative natural SUSY with a 125 GeV Higgs boson," *Phys.Rev.Lett.* **109** (2012) 161802, [arXiv:1207.3343 \[hep-ph\]](#). ; H. Baer, V. Barger, P. Huang, D. Mickelson, A. Mustafayev, *et al.*, "Radiative natural supersymmetry: Reconciling electroweak fine-tuning and the Higgs boson mass," [arXiv:1212.2655 \[hep-ph\]](#). ; P. Lodone, "Supersymmetry phenomenology beyond the MSSM after 5/fb of LHC data," *Int.J.Mod.Phys.* **A27** (2012) 1230010, [arXiv:1203.6227 \[hep-ph\]](#). ; H. M. Lee, V. Sanz, and M. Trott, "Hitting sbottom in natural SUSY," *JHEP* **1205** (2012) 139, [arXiv:1204.0802 \[hep-ph\]](#). ; M. Perelstein and B. Shakya, "XENON100 Implications for Naturalness in the MSSM, NMSSM and lambda-SUSY," [arXiv:1208.0833 \[hep-ph\]](#). ; E. Hardy, "Is Natural SUSY Natural?," [arXiv:1306.1534 \[hep-ph\]](#).
- [15] M. Blanke, G. F. Giudice, P. Paradisi, G. Perez, and J. Zupan, "Flavoured Naturalness," *JHEP* **1306** (2013) 022, [arXiv:1302.7232 \[hep-ph\]](#).
- [16] O. Buchmueller and J. Marrouche, "Universal mass limits on gluino and third-generation squarks in the context of Natural-like SUSY spectra," [arXiv:1304.2185 \[hep-ph\]](#).

- [17] G. D. Kribs, A. Martin, and A. Menon, “Natural Supersymmetry and Implications for Higgs physics,” [arXiv:1305.1313 \[hep-ph\]](#).
- [18] G. L. Kane, C. F. Kolda, L. Roszkowski, and J. D. Wells, “Study of constrained minimal supersymmetry,” *Phys.Rev.* **D49** (1994) 6173–6210, [arXiv:hep-ph/9312272 \[hep-ph\]](#).
- [19] **CMS** Collaboration, S. Chatrchyan *et al.*, “Interpretation of searches for supersymmetry with simplified models,” [arXiv:1301.2175 \[hep-ex\]](#).
- [20] **CMS** Collaboration, S. Chatrchyan *et al.*, “Search for supersymmetry in hadronic final states with missing transverse energy using the variables α_T and b-quark multiplicity in pp collisions at $\sqrt{s} = 8$ TeV,” [arXiv:1303.2985 \[hep-ex\]](#).
- [21] “Search for direct ewk production of susy particles in multilepton modes with 8tev data,” Tech. Rep. CMS-PAS-SUS-12-022, CERN, Geneva, 2012
- [22] A. Fowlie, A. Kalinowski, M. Kazana, L. Roszkowski, and Y. S. Tsai, “Bayesian Implications of Current LHC and XENON100 Search Limits for the Constrained MSSM,” *Phys.Rev.* **D85** (2012) 075012, [arXiv:1111.6098 \[hep-ph\]](#).
- [23] A. Fowlie, M. Kazana, K. Kowalska, S. Munir, L. Roszkowski, *et al.*, “The CMSSM Favoring New Territories: The Impact of New LHC Limits and a 125 GeV Higgs,” *Phys.Rev.* **D86** (2012) 075010, [arXiv:1206.0264 \[hep-ph\]](#).
- [24] K. Kowalska, S. Munir, L. Roszkowski, E. M. Sessolo, S. Trojanowski, *et al.*, “The Constrained NMSSM with a 125 GeV Higgs boson – A global analysis,” *Phys. Rev.* **D87** (2013) 115010, [arXiv:1211.1693 \[hep-ph\]](#).
- [25] K. Kowalska, L. Roszkowski, and E. M. Sessolo, “Two ultimate tests of constrained supersymmetry,” *JHEP* **1306** (2013) 078, [arXiv:1302.5956 \[hep-ph\]](#).
- [26] “Search for direct top squark pair production in final states with one isolated lepton, jets, and missing transverse momentum in $\sqrt{s} = 8$ TeV pp collisions using 21 fb⁻¹ of atlas data,” Tech. Rep. ATLAS-CONF-2013-037, CERN, Geneva, Mar, 2013
- [27] S. P. Martin, “A Supersymmetry primer,” [arXiv:hep-ph/9709356 \[hep-ph\]](#).
- [28] P. J. Fox, A. E. Nelson, and N. Weiner, “Dirac gaugino masses and supersoft supersymmetry breaking,” *JHEP* **0208** (2002) 035, [arXiv:hep-ph/0206096 \[hep-ph\]](#).
- [29] **Particle Data Group** Collaboration, J. Beringer *et al.*, “Review of Particle Physics (RPP),” *Phys.Rev.* **D86** (2012) 010001.
- [30] **Planck** Collaboration, P. Ade *et al.*, “Planck 2013 results. XVI. Cosmological parameters,” [arXiv:1303.5076 \[astro-ph.CO\]](#).
- [31] **WMAP** Collaboration, E. Komatsu *et al.*, “Seven-Year Wilkinson Microwave Anisotropy Probe (WMAP) Observations: Cosmological Interpretation,” *Astrophys. J. Suppl.* **192** (2011) 18, [arXiv:1001.4538 \[astro-ph.CO\]](#)
- [32] H. Baer and J. List, “Post LHC8 SUSY benchmark points for ILC physics,” [arXiv:1307.0782 \[hep-ph\]](#).

- [33] B. Allanach, “SOFTSUSY: a program for calculating supersymmetric spectra,” *Comput.Phys.Commun.* **143** (2002) 305–331, [arXiv:hep-ph/0104145](#) [hep-ph].
- [34] A. Arbey and F. Mahmoudi, “SuperIso Relic: A program for calculating relic density and flavor physics observables in Supersymmetry,” *Comput.Phys.Commun.* **176** (2007) 367–382, [arXiv:0906.0369](#) [hep-ph].
- [35] G. Belanger, F. Boudjema, A. Pukhov, and A. Semenov, “micrOMEGAs2.0: a program to calculate the relic density of dark matter in a generic model,” *Comput.Phys.Commun.* **181** (2010) 1277–1292, [arXiv:hep-ph/0607059](#) [hep-ph].
- [36] A. Djouadi, M. Muhlleitner, and M. Spira, “Decays of supersymmetric particles: The Program SUSY-HIT (SUSpect-SdecaY-Hdecay-InTerface),” *Acta Phys.Polon.* **B38** (2007) 635–644, [arXiv:hep-ph/0609292](#) [hep-ph].
- [37] T. Sjostrand, S. Mrenna, and P. Z. Skands, “PYTHIA 6.4 Physics and Manual,” *JHEP* **0605** (2006) 026, [arXiv:hep-ph/0603175](#) [hep-ph].
- [38] <http://physics.ucdavis.edu/~conway/research/software/pgs/pgs4-general.htm>
- [39] CMS Collaboration, S. Chatrchyan *et al.*, “Search for new physics in events with same-sign dileptons and b jets in pp collisions at $\sqrt{s} = 8$ TeV,” *JHEP* **1303** (2013) 037, [arXiv:1212.6194](#) [hep-ex].
- [40] <https://twiki.cern.ch/twiki/bin/view/AtlasPublic/FlavourTaggingPublicResultsCollisionData>
- [41] <https://twiki.cern.ch/twiki/bin/view/LHCPhysics/SUSYCrossSections>
- [42] “Search for electroweak production of charginos, neutralinos, and sleptons using leptonic final states in pp collisions at 8 tev,” Tech. Rep. CMS-PAS-SUS-13-006, CERN, Geneva, 2013
- [43] “Search for direct production of the top squark in the all-hadronic $t\bar{t}$ + $e\text{miss}$ final state in 21 fb⁻¹ of p - p collisions at $\sqrt{s}=8$ tev with the atlas detector,” Tech. Rep. ATLAS-CONF-2013-024, CERN, Geneva, Mar, 2013
- [44] “Search for direct third generation squark pair production in final states with missing transverse momentum and two b -jets in $\sqrt{s} = 8$ tev pp collisions with the atlas detector,” Tech. Rep. ATLAS-CONF-2013-053, CERN, Geneva, May, 2013
- [45] “Search for top-squark pair production in the single lepton final state in pp collisions at 8 tev,” Tech. Rep. CMS-PAS-SUS-13-011, CERN, Geneva, 2013
- [46] “Search for direct top squark pair production in final states with two leptons in $\sqrt{s} = 8$ tev pp collisions using 20fb⁻¹ of atlas data.,” Tech. Rep. ATLAS-CONF-2013-048, CERN, Geneva, May, 2013
- [47] “Search for direct production of charginos and neutralinos in events with three leptons and missing transverse momentum in 21 fb⁻¹ of pp collisions at $\sqrt{s} = 8$ tev with the atlas detector,” Tech. Rep. ATLAS-CONF-2013-035, CERN, Geneva, Mar, 2013

- [48] “Search for direct-slepton and direct-chargino production in final states with two opposite-sign leptons, missing transverse momentum and no jets in 20/fb of pp collisions at $\sqrt{s} = 8$ tev with the atlas detector,” Tech. Rep. ATLAS-CONF-2013-049, CERN, Geneva, May, 2013
- [49] https://twiki.cern.ch/twiki/pub/CMSPublic/PhysicsResultsSUS12028/SUS-12-028_result.pdf
- [50] **CMS** Collaboration, S. Chatrchyan *et al.*, “Search for gluino mediated bottom- and top-squark production in multijet final states in pp collisions at 8 TeV,” [arXiv:1305.2390 \[hep-ex\]](#).
- [51] “Search for strongly produced superpartners in final states with two same sign leptons with the atlas detector using 21 fb-1 of proton-proton collisions at $\sqrt{s}=8$ tev.,” Tech. Rep. ATLAS-CONF-2013-007, CERN, Geneva, Mar, 2013
- [52] “Search for supersymmetry in pp collisions at $\sqrt{s} = 8$ tev in events with three leptons and at least one b-tagged jet,” Tech. Rep. CMS-PAS-SUS-13-008, CERN, Geneva, 2013
- [53] “Search for supersymmetry in pp collisions at 8 tev in events with a single lepton, multiple jets and b-tags,” Tech. Rep. CMS-PAS-SUS-13-007, CERN, Geneva, 2013
- [54] “Search for squarks and gluinos with the atlas detector in final states with jets and missing transverse momentum and 20.3 fb⁻¹ of $\sqrt{s} = 8$ tev proton-proton collision data,” Tech. Rep. ATLAS-CONF-2013-047, CERN, Geneva, May, 2013
- [55] N. Arkani-Hamed, A. Delgado, and G. Giudice, “The Well-tempered neutralino,” *Nucl.Phys.* **B741** (2006) 108–130, [arXiv:hep-ph/0601041 \[hep-ph\]](#).
- [56] H. Baer, V. Barger, and D. Mickelson, “Direct and indirect detection of higgsino-like WIMPs: concluding the story of electroweak naturalness,” [arXiv:1303.3816 \[hep-ph\]](#).
- [57] **XENON100** Collaboration, E. Aprile *et al.*, “Dark Matter Results from 225 Live Days of XENON100 Data,” *Phys.Rev.Lett.* **109** (2012) 181301, [arXiv:1207.5988 \[astro-ph.CO\]](#).
- [58] **LUX** Collaboration, D. Akerib *et al.*, “The Large Underground Xenon (LUX) Experiment,” *Nucl.Instrum.Meth.* **A704** (2013) 111–126, [arXiv:1211.3788 \[physics.ins-det\]](#).
- [59] **XENON1T** Collaboration, E. Aprile, “The XENON1T Dark Matter Search Experiment,” [arXiv:1206.6288 \[astro-ph.IM\]](#).
- [60] “Search for electroweak production of supersymmetric particles in final states with at least two hadronically decaying taus and missing transverse momentum with the atlas detector in proton-proton collisions at $\sqrt{s} = 8$ tev,” Tech. Rep. ATLAS-CONF-2013-028, CERN, Geneva, Mar, 2013